Electrochimica Acta 441 (2023) 141860

Contents lists available at ScienceDirect

Electrochimica Acta

journal homepage: www.journals.elsevier.com/electrochimica-acta

Promising sustainable technology for energy storage devices: Natural protein-derived active materials

Chenxu Wang, Wei-Hong Zhong *

School of Mechanical and Materials Engineering, Washington State University, Pullman, WA 99164, USA

ARTICLE INFO

Keywords:
Protein
Active material
Electrode
Electrochemical
Energy storage
Battery
Supercapacitor
Catalyst
Genetical engineering

ABSTRACT

Electrochemical energy storage devices (EESDs) are critical technologies in modern economy, covering numerous fields such as portable electronics, electric vehicles, etc. The expanding market of EESDs demands for extra requirements such as safety, environmental friendliness and low cost, in addition to increasingly enhanced electrochemical properties. Natural proteins are abundant, versatile bio-macromolecules involving tremendous amount of amino acids/functional groups/heteroatoms, which greatly benefit sustainable technologies for advancing performances of EESDs. Recent years, significant research on utilizing natural proteins including plant/animal proteins to fabricate active materials for enhancing performance of EESDs has been well reported. Therefore, it is important to comprehensively summarize the progress and achievements, analyze the advantages/challenges, and predict the prospective for future protein-based strategies toward high-performance EESDs, which are the contents of this review. The protein-derived active materials include activated carbons, silicon, sulfur, metal alloys, transitional metal compounds, and nonprecious metal catalysts. The resulting EESDs are associated with Li-/Na-/K-ion batteries, metal–air batteries, and redox flow batteries, as well as supercapacitors. The contributions of proteins to stabilizing/protecting electrodes, and thus enhancing performance of EESDs are specifically emphasized. Furthermore, studies on genetical engineering of proteins for directing self-assembly of active material nanoparticles are introduced.

Abbreviations: EESD, Electrochemical energy storage device; EVs, electric vehicles; SSA, specific surface area; ORR, oxygen reduction reaction; OER, oxygen evolution reaction; EC, ethylene carbonate; EMC, ethyl methyl carbonate; DMC, dimethyl carbonate; DEGDME, tetra (ethylene) glycol dimethyl ether); FEC, fluoroethylene carbonate; VRFB, vanadium redox flow battery; SEM, scanning electron microscope. FE-SEM, field emission scanning electron microscopes; XPS, X-ray photoelectron spectroscopy; EDS, energy-dispersive X-ray spectroscopy; TEM, transmission Electron Microscopy; Lys, lysine; Trp, tryptophan; Phe, phenylalanine; PP, polypropylene; PE, polyethylene; PVA, poly(vinyl alcohol); DEC, diethyl carbonate; DOL, dioxolane; DME, dimethoxyethane; AEMFCs, anion exchange membrane Fuel Cells; PQQ-GDH, pyrroloquinoline quinone-dependent glucose dehydrogenase; Gr, graphene; OCV, open circuit potential; NiFe-LDH, NiFe layered double hydroxide; RHE, reversible hydrogen electrode; Cys, cysteine; TMV, Tobacco mosaic virus; SEI, solid electrolyte interphase; BSA, bovine serum albumin; PAA, polyacrylic acid; CE, Coulombic efficiency; M-N/C, transition metal–nitrogen/carbon; MO, manganese oxide. SWNTs, single-wall carbon nanotubes; TEGDME, tetraethylene glycol dimethyl ether. PC, propylene carbonate; ELP, elastin-like polypeptides; $TEABF_4$, Tetraethylammonium tetrafluoroborate; AN, acetonitrile; $EMIMBF_4$, 1-Ethyl-3-methylimidazolium tetrafluoroborate; SPI, soy protein isolate

1. Introduction: why natural proteins favorable to electrochemical energy storage systems?

Electrochemical energy storage devices (EESDs) are the systems of storing and releasing energy by electricity through reversible electrochemical processes with high energy utilization efficiency [1]. In the past decades, more and more significant electrochemical energy storage technologies have been developed for portable electronics, electric vehicles (EVs), and renewable power plants, which demand for EESDs with different performance requirements [2]. For example, the batteries for portable phones and laptops particularly require properties including minimizing, lightweight, high energy density and long cycling life [3]. The expanding market of EVs demands battery packages or hybrid EESDs with increasingly high power/energy density, safety and rate-cycling performance, etc. [4]. Moreover, for the grid-scale

* Corresponding author.
E-mail address: katie_zhong@wsu.edu (W.-H. Zhong).

https://doi.org/10.1016/j.electacta.2023.141860
Received 2 September 2022; Received in revised form 4 January 2023; Accepted 5 January 2023
Available online 7 January 2023

stationary storage systems serving power plants, the raw material cost of the unit energy capacity is one of the most critical parameters for practical applications. Nowadays, the conventional EESDs have the shortcomings of either safety issues, high manufacturing costs, poor cycling performance, or unsatisfactory energy/power densities [5,6]. To solve these issues, the development of high-performance electrodes by creating active materials with effective physicochemical properties becomes one of the critical strategies to obtain high-performance EESDs.

Two mainstream EESDs are batteries and supercapacitors; each has a sandwich structure composed of two electrodes and a separator within the container filled with electrolytes. The electrode sheets are usually prepared by coating slurries on current collectors. The slurry consists of active materials, binders and conductive agents in a solvent that can keep the homogenous suspension state for the slurry. Among the compositions of an electrode, dominant amount of active materials of electrode components, i.e. high ratios of active materials over the binder and conductive agents, is desirable for maximizing the energy density of electrodes. Moreover, big surface areas coming from small sizes/miniatured structures of the active material particles are responsible for high efficiency of active material utilization leading to improved performance of electrodes. Therefore, constructing active material nanostructures with large specific surface areas (SSAs) and high ionic/electronic conductivity is expected to be a promising approach to improving the overall performance of electrodes for EESDs.

Batteries are charged/discharged by two reversible half-reactions in the cathode and anode. During the cycling processes, the ions transfer between electrodes and have a slow reaction rate in the electrodes. The slow reactions are derived from limited ion diffusion and inefficient electron transfer in active material particles. Hence, the batteries suffer from low power density although they may have high energy densities. There are many kinds of batteries with various performances dependent on their chemical components and structures of active materials in anode/cathodes. The most commercial rechargeable batteries are Li-ion batteries, in which the graphite anode has stable cycling performance but low specific capacity (372 mAh g^{-1}). The alternative anodes with higher specific capacities, e.g., Si (4200 mAh g^{-1}), Sn (994 mAh g^{-1}) and transitional metal oxides (SnO_2, Fe_2O_3, NiO) are plagued by the short cycle lifespan due to the volume-change-induced electrode pulverization [7–11]. The applications of Li-ion batteries are widely found in portable devices (e.g., phones, laptops, etc.) without high-power-density demand; while EVs need a bulk battery management system to monitor/control the battery pack. The batteries using other metal-based anodes (e.g., K and Na) have various shortcomings such as short lifespan and low energy/power density. The metal–air batteries (e.g., Li- and Zn–air) release and store electrical energy by the oxygen reduction reaction/oxygen evolution reaction (ORR/OER) in the air cathode [12]. In metal–air batteries, the activity of electrocatalysts is closely related to the kinetic reaction rate of ORR/OER during cycling. The rechargeable flow batteries, specifically, low-cost vanadium redox flow batteries (VRFBs) need large space to accommodate the electrolyte tank, which can attach as the grid energy storage for power plants [13]. Similar to that of metal–air batteries, the energy conversion efficiency and storage capacity of VRFBs are also highly affected by electrocatalyst active materials in the cathodes. To improve the energy density and lifespan of batteries, it is important to design active materials with high specific capacities, stable structures and/or high catalytic activity.

Supercapacitors are advanced capacitors absorbing and generating electrical energy *via* ion transfer in electrolytes and absorption/desorption on electrode surfaces during charge/discharge processes. Supercapacitors can be fully charged within a short time and release electrical energy with high Coulombic efficiency (CE) of ~100% and a high-power output for over 10, 000 cycles [14]. Thus, supercapacitors have been widely applied as EESDs for high-power-output demanding devices such as electrical drills, acceleration and brake systems for EVs. The two symmetrical electrode layers in conventional supercapacitors can store/release electrolyte ions during cycling processes. The electrode surfaces, including the inner surface of pores in electrode active materials, form an electric double layer at the charge state. Therefore, the material with a high specific surface area (SSA) can provide high capacitance. Typical materials with high SSAs, such as graphene sheets, mesoporous activated carbons and carbon nanotubes, have been used as the symmetrical electrodes of supercapacitors [15–17]. Another type of supercapacitors, pseudocapacitors, which are based on hybrid mechanisms of ion storing/absorbing in both batteries and capacitors, have reduction/oxidation reactions of electrolyte ions in the electrodes and part of ions absorb/desorb on the electrode surfaces. The typical active materials for pseudocapacitors include RuO_2, NiS, $Ni(OH)_2$, etc. [18–21]. Pseudocapacitors have a relatively high energy density compared to supercapacitors and high-power output compared to batteries. To increase the capacitance of the above two types of supercapacitors, numerous efforts on creating porous nanostructures of active materials with high SSAs have been widely reported.

Natural proteins are versatile macromolecules, composed of multiple polypeptides with folded structures containing vast arrays of various amino acids formed over long-time evolution. In polypeptides, there are tremendous amount of functional groups with numerous heteroatoms, which are responsible for transport of various metallic ions/nutrition compounds necessary for organisms. These transport mechanisms can be utilized to advance performance of EESDs as the functional groups incur interactions with ions, charged/non-charged atoms, and/or polar/non-polar chemical groups [22]. Proteins may help form desirable material surfaces and structures for electrodes of EESDs [23–25]. Natural proteins exist with folded quaternary structures embedding the functional groups due to the strong intermolecular interactions. To unfold the protein structures and build desired physicochemical properties of protein structures, appropriate denaturation processes are applied to break down the interactions for exposing more functional groups, such as polar and non-polar groups, etc. Hence, after controlled denaturation processes, proteins can show great potential to build interactions with polymers, metal atoms, ions, or solvent molecules [26]. The increasing efforts on protein-derived materials with a specific configuration of nanostructure inspired the development of active materials for ESSDs. For example, proteins contain rich N, O, S and a huge amount of binding sites for organic/inorganic materials as well as metal ions, thus can be carbonized and activated to a rich heteroatom-doped porous carbon with high SSAs [27,28]. In addition, the specific configurations of proteins also induce various atom arrangements of materials, which can be used to template nanoparticle assemblies. These applications were derived from the exposed functional groups and specific molecular structures after denaturation in various solvents (e.g., ethanol, acetic acid, etc.) [29]. These reported studies demonstrated the effectiveness of proteins for the electrode performance improvement of EESDs.

Most studies of protein-derived materials were limited within the fields of medicine, sensor and disposable materials. Recent years, significant studies on application of proteins in EESDs, in particular, on electrode with protein-derived active materials, have been reported. It is important to comprehensively summarize the progress and achievements, analyze the advantages, and predict the perspectives for future protein-based strategies toward high-performance EESDs electrodes.

In this review, we summarize the methods of synthesizing various protein-derived active materials for electrodes, and make a comprehensive comparison of the performance in different EESDs.

The electrodes with proteins involved can be categorized into two types, including protein-derived carbons and protein-modified active materials (Fig. 1). The protein-derived carbons can be prepared by a carbonization method and followed by an activation process of pyrolysis, which is summarized in Section 2. The activated carbons derived from proteins possess heteroatom-doping and hierarchical porous nanostructures with various dimensions such as nanosphere, nanorod, nanosheet and interconnected 3D structures. In Section 3, reported studies on modifications of active materials by using proteins are summarized. The basic mechanisms are based on the rich functional groups

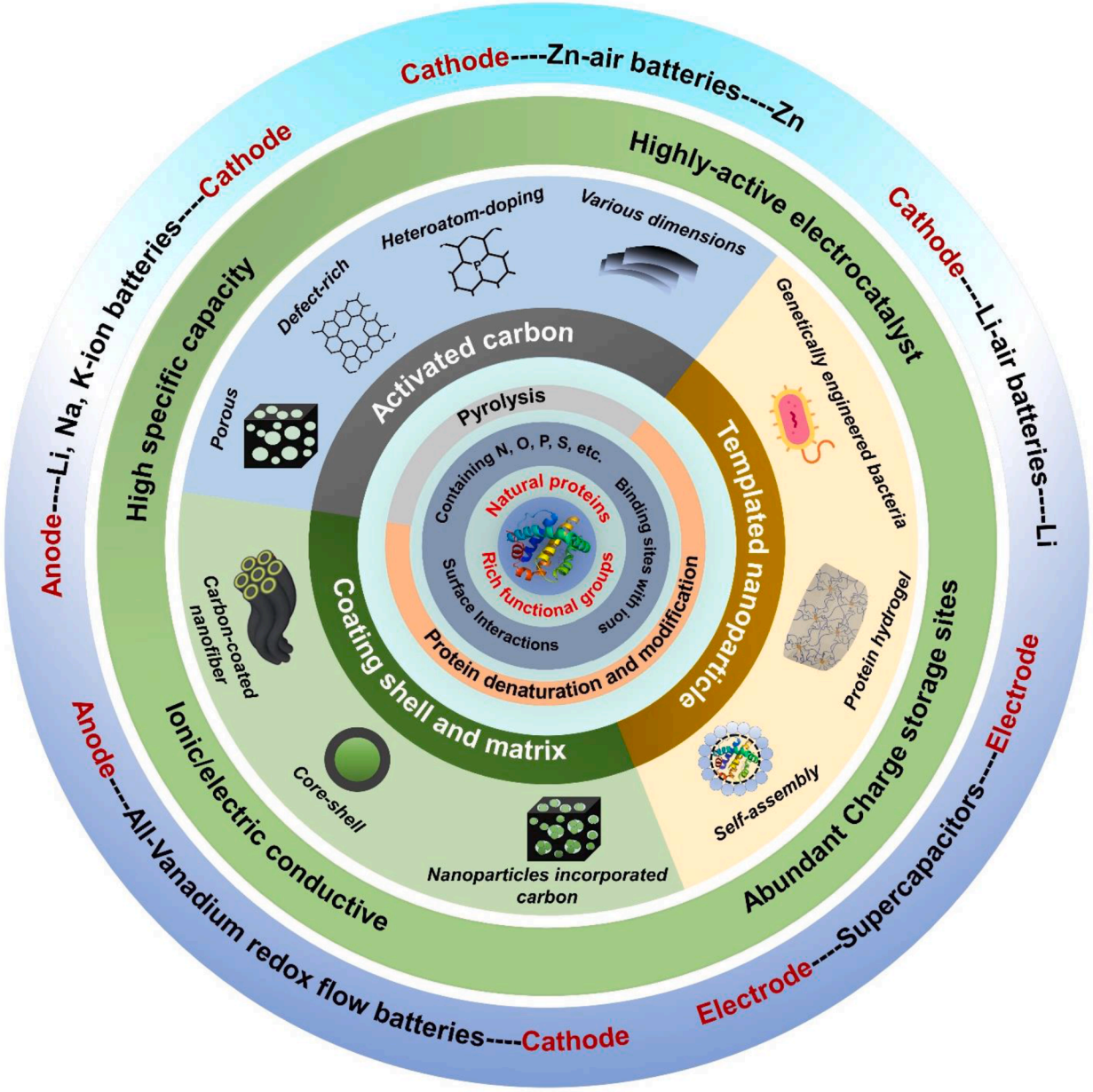

Fig. 1. Schematic of protein-derived active materials for electrodes of electrochemical energy storage devices (EESDs).

exposed on the protein structures after appropriate denaturation. The protein-modified materials can be divided into templated nanoparticles and active materials with a coating or matrix. (1) Templated nanoparticles: with protein as a self-sacrificing template for the formation and growth of nanoparticles, the resultant active materials have various nanostructures. (2) Active materials with a coating or matrix: the absorption of protein molecules on nanoparticles forms a protein coating layer, which can be carbonized after a calcination process. Moreover, protein modulation on the self-assembly behavior of particles was used to generate nanoparticle-incorporated carbon matrices. Moreover, in Section 4, the genetically engineered bacteria/viruses with tuneable protein coats were used to template the formation of hollow sphere nanostructures; protein hydrogels help generated the highly dispersed nanospheres; protein molecules modulated self-assembly of nanoparticles to form different architectures of macroparticles.

2. Protein-derived activated carbons

Activated carbons are widely applied as active materials in EESDs due to the low cost and multifunctionalities derived from the morphology diversity and various chemical constituents. In specific, activated carbons with mesoporous structures bring about the advantage of large SSAs that provide ionic transfer channels and good wetting with electrolytes. With various raw materials and different activation processes, activated carbons with tunable pore sizes and chemical constituents are fabricated. The activated carbons are used as the active materials or electrocatalysts in batteries, including metal–ion batteries, metal–air batteries, and redox flow batteries, as well as supercapacitors.

Natural proteins, are used as the raw materials to create heteroatom-doped activated carbons due to their rich contents of N, O and S, etc. existing in their tremendous amount of various amino acids. The proteins used for synthesizing activated carbons can be categorized into animal proteins (e.g., silk, egg white, milk, etc.) and plant proteins (e.g., soy, zein, wheat, etc.). (1) Silk protein: silk is a protein fibric composed

of fibroin and sericin, and is produced from insect cocoons. The silk with a thermally transformation can generate the pyroprotein possessing a good thermostability. (2) Egg white: egg white is the solution containing ~90% water and ~10% proteins. The primary proteins of egg white are ovalbumin (54%), ovotransferrin (12%), ovomucoid (11%) and ovomucin (3.5%). (3) Milk: casein (~80%) and whey protein (~20%) are the two main proteins of milk. (4) Soy protein: soy protein is widely studied and used in numerous food products such as tofu, soy meal, soybean, soy flour and soy protein isolate. (5) Zein/corn protein: zein is a corn protein that has been heavily studied to synthesize fibric by using electrospinning. (6) Wheat protein: wheat protein comprised of gliadin and glutenin can enhance the elasticity of food (e.g., noodles) in the application of food products. The morphology and chemical constituents of protein-derived activated carbons can be modulated by the raw materials, protein denaturation agents, solvents, dry processes and activation agents/temperatures. The reported performances of protein-derived activated carbons for EESDs are summarized in Table 1.

2.1. Anodes for Li-, K- and Na-ion batteries

Proteins are a promising natural source for the fabrication of heteroatoms co-doped activated carbons due to their rich contents of N, O, S atoms. Protein-derived activated carbons have been studied as the anodes for Li-ion batteries. The reported major protein materials used as precursor of activated carbons in Li-, K- and Na-ion batteries are soy protein, reed catkins, egg white and silk.

Firstly, more studies on protein-derived activated carbons were reported for electrodes of Li-ion batteries. For example, a hierarchical porous carbon material was prepared by a combination of freeze-drying (−55 °C) and carbonization (800 °C for 3 h in Ar) processes using egg white protein as the raw material and NaCl as the denaturation agents [33,34]. As shown in Fig. 2**a**, the pore size distribution of the resultant carbons was rationally tailored by controlling the salt concentration in the protein solutions. The salt concentration was optimized at 4 M for obtaining a honeycomb-like mesoporous network structure that possesses high SSAs and good cycling capacity. The same synthesis process was also applied by using soy protein to prepare an ultra-thin carbon nanosheet with N doping [30]. As shown in Fig. 2**b**, various carbon sheets were fabricated by controlling concentrations of denaturation agent (NaCl) and carbonization temperatures to tailor SSAs and pore structures. When applied in the anode of Li-ion batteries, the carbon sheet prepared at 600 °C showed a high reversible capacity of 1084 mAh g^{-1} in the 100th cycle at 0.05 A g^{-1}.

Another typical example of protein-derived activated carbons for Li-ion batteries was fabricated using soy protein as the carbon source. Soybean was treated by a facile dry process to obtain the N-doped porous carbon as shown in Fig. 2c [31]. In specific, soybean was dry mixed with the activation of KOH, and then the mixture was carbonized at the temperature range of 300–800 °C. The obtained carbon formed an interconnected 3D framework with generated graphitic nanocrystals and doped N atoms (Fig. 2**d**), exhibiting a large SSA of 1089.84 $m^2 g^{-1}$. These properties enhanced the cycling performance of the obtained carbon to 360 mA h g^{-1} in the 100th cycle at a current density of 0.5 C.

In addition, a protein-containing plant, reed catkins (a slim flower cluster of reeds), as a carbon precursor to form N-doped porous carbon tubes for electrode of Li-ion batteries was reported. In the study, $ZnCl_2$ was used as the activation agent, and the results showed an improved specific capacity of 1123.1 mA h g^{-1} at 0.02 A g^{-1} in Li-ion batteries [32].

For application in Na-, K-ion batteries, protein-derived activated carbons were also prepared for use as the anode materials. Pyroprotein, a silk-transformed protein with good thermostability, was carbonized at an extremely high temperature (2000 °C) without salt activation, forming low-density carbon fibers with multitudinous closed pores (small nanometer scale), which were used as the anode for Na-ion batteries [35]. The pyroprotein-dervied carbon fibers showed a superior capacity of 300 mA h g^{-1} at ~0.1 V (vs. Na^+/Na) and a high initial CE of ~91.9%. Silk fibers of cocoon were used as the precursor to synthesize N-doped carbon micro-rods with enlarged interlayer spacing [36]. When employed as the anode of Na-ion batteries, the activated carbon exhibited excellent cycling stability of 161.5 mAh g^{-1} at 2 A g^{-1} after 5000 cycles. In K-ion batteries, the activated carbon derived from protein (the authors didn't indicate the type of protein.) built a high capacity of 132 mA h g^{-1} at 9.6 A g^{-1} and 0.02% capacity decay per cycle over 1000 cycles at 3 A g^{-1} [37].

2.2. Cathode electrocatalysts for metal–air batteries

Heteroatom-doped activated carbon is an important type of cathode electrocatalysts that were developed to obtain superior electrocatalytic activity and stability in metal–air batteries. Soy and silk proteins were primarily used for fabricating carbon electrocatalysts of metal–air batteries. For example, a soy protein-derived porous carbon by using tofu and activation via KOH was used as the cathode electrocatalyst in Li–air batteries [38]. The activated carbon not only exhibited excellent cycling stability of 1000 mAh g^{-1} at the 25th cycle, but also showed a low overpotential of 1.54 V. In another study, a silk-derived defect-rich and N-doped porous nanocarbon was employed as the cathode electrocatalysts of Zn–air batteries for improving the activity of ORR/OER [39]. In the preparation process, Ketjenblack (a unique electro-conductive carbon black) was impregnated into silk fiber solution, modulating the thickness and increasing the rich edge defects in the silk-derived carbon (Fig. 3**a**). The scanning electron microscopy (SEM) image of the resulting carbon displayed a high interconnected-nanoparticle structure (Fig. 3**b**). The transmission electron microscopy (TEM) result demonstrated the rich defects (amorphous structure) that are beneficial to the electrocatalytic performance of catalysts (Fig. 3**c**). N- and O-doped situations were calculated from the X-ray photoelectron spectroscopy (XPS), which revealed the rich dope contents of N (0.83 at.%) and O (1.63 at.%) (Fig. 3**d**). In the electrochemical performance results, the nanocarbon electrocatalysts exhibited a remarkable ORR catalytic activity (onset potential = 0.95 V), a small current density (6.34 mA cm^{-2}), a Tafel slope of 68 mV dec^{-1} and high stability with only 30 mV loss in its half-wave potential after accelerated degradation test for 50, 000 cycles (vs. 47 mV loss of Pt/C catalyst in its half-wave potential after only 5000 cycles). In a study of an electrocatalyst for Zn-air batteries, legume root nodule, a plant with rich iron-containing protein (leghaemoglobin), was used as the precursor of activated carbon *via* the activation of $ZnCl_2$ salt at a temperature range of 700–1000 °C [40]. This study provides a simple strategy to synthesize in situ S, N, Mo, and Fe-doped carbon-based catalysts with high SSAs. As shown in Fig. 3**e, f**, with metal atoms in polypeptide chains, the protein generated homogenously dispersed clusters of metal/metal compound (Fe and MoFe) in the synthesized porous carbon, and thus, improving the electrocatalyst performance.

2.3. Electrodes of redox flow batteries

The electrochemistry reactions in VRFBs happen on the surface of electrocatalyst particles (such as noble/transition metals and carbon), realizing the transformation between chemical energy and electric energy. To enhance the performance of VRFBs, an electrode with a 3D structure (facilitating flow of electrolyte) and a large SSA (providing a large reaction area) are desirable to decrease the over-potential of redox reactions and increase the electrical conductivity.

Thus far, silk protein was primarily reported for synthesizing activated carbon for electrocatalyst of VRFBs. The silk-derived carbon fibers carbonized at different temperatures was employed as the electrodes for VRFBs (Fig. 4**a**) [41]. In specific, cocoon was firstly dipped into boiled solution of Na_2CO_3 to remove impurities and sericin (one protein of silk). After drying, the resulting silk fibers were pyrolyzed in argon atmosphere at the temperature of 800–2800 °C, respectively. The SEM and

Table 1
Protein-derived carbon active materials for EESDs.

Protein type	Carbon type	SSA ($m^2\ g^{-1}$)	Activation agent	System	Electrochemical performance	Electrolyte	Counter Electrode	Ref.
Soy	Carbon nanosheets	550	NaCl	Li-ion	355 mAh g^{-1} at 1 A g^{-1} after 1000 cycles	1 M $LiPF_6$ in EC/EMC/DMC	Li	[30]
Soy	Porous honeycomb-like carbon	1089.8	KOH	Li-ion	275 mA h g^{-1} at 4 C after 1000 cycles	1 M $LiPF_6$ in EC/ DMC	Li	[31]
Reed catkins	Carbon Tubes	1751.1	$ZnCl_2$	Li-ion	512.4 mA h g^{-1} after 500 cycles at 1 A g^{-1}	1 M $LiPF_6$ in EC/ DMC	Li	[32]
Egg white	Hierarchical porous carbon	1745.6	NaCl	Li-ion	355 mAh g^{-1} at 1 A g^{-1} after 1000 cycles	1 M $LiPF_6$ in EC/EMC/DMC	Li	[33]
Egg white	Cheese-like bulk carbon	360.6	None	Li-ion & Na-ion	470 mA h g^{-1} (Li) & ~35 mA h g^{-1} (Na) after 100 cycles at 5 mA g^{-1}	1 M $LiPF_6$ in EC/ DMC & 1 M $NaPF_6$ in EC/DMC	Li & Na	[34]
Silk (pyroprotein)	Hard-carbon fiber	6.3	None	Na-ion	70 mA h g^{-1} at 20 mA g^{-1}	1 M $NaPF_6$ in DEGDME	$Na_{1.5}VPO_{4.8}F_{0.7}$	[35]
Silk	Carbon micro-rods	No indication	None	Na-ion	161.5 mAh g^{-1} at 2 A g^{-1} for over 5000 cycles	1 M $NaClO_4$ in EC/DEC with 2% FEC	Li	[36]
No indication	3D amorphous carbon	181.9	NaCl	K-ion	132 mA h g^{-1} at 9.6 A g^{-1}	0.8 M KPF_6 in EC/DEC	K	[37]
Soy (Tofu)	N,P co-doped porous activated carbon	2473.3	KOH	Li-air	3724 mA h g^{-1} at 100 mA g^{-1}	1.0 LiTFSI TEGDME	Li	[38]
Silk	Defect-rich and N-doped carbon	847.43	None	Zn-air	Voltage gap = 1.39 V, voltaic efficiency = 41.3% after 100 cycles	6.0 M KOH + 0.2 M ZnAC, PVA aquous gel	Zn	[39]
Soy (root nodule)	Fe, Mo, S, N self-doped porous carbon	1835	$ZnCl_2$	Zn-air	Half-wave potentials of 0.723 V and 0.868 V (vs. RHE) in 0.1 M $HClO_4$ and 0.1 M KOH solution	6 M KOH + 0.2 M Zn $(CH_3CO_2)_2$	Zn	[40]
Silk	Carbon fabrics	5.1	None	VRFB	Energy efficiency = 86.8%	1.6 M $VOSO_4$ in 4 M H_2SO_4 solution	Symmetrical	[41]
Silk (twin cocoon)	Self- standing monolithic carbon	21.16	None	VRFB	50% redox potential decrease & 192% diffusion slope increase	1.0 M $VOSO_4$ + 3.0 M H_2SO_4	Pt, Ag/AgCl	[42]
Casein (milk)	Porous hybrid carbon	2050.5	KOH	Supercapacitor	358.4 F g^{-1} at 0.1 A g^{-1}	6 M KOH	Symmetrical	[43]
Soy	P and N co-doped carbon	Not provided	None	Supercapacitor	127 F g^{-1}	1 M H_2SO_4	Ag/AgCl & Hg/HgO	[44]
Soy (tofu)	Protein isolate porous carbon	1727.54	KOH	Supercapacitor	280F g^{-1}	6 M KOH	Three electrodes	[45]
Soy (SPI)	N-doped carbon aerogels	726.84	KOH	Supercapacitor	231.75 F g^{-1} at 0.5 A g^{-1}, 85.7% retention after 5000 cycles	6 mol L^{-1} KOH	Three electrodes	[46]
Soy	In-situ N-doped activated carbon	558.2	CO_2	Supercapacitor	106 F g^{-1} at 0.25 A g^{-1}, 93% retention at 10 A g^{-1} after 20,000 cycles	6 M KOH	symmetrical	[47]
Soy	N, O, P, S-doped porous carbon	2959	KOH	Supercapacitor	685.1 F g^{-1} at 0.5 A g^{-1}, 80% retention after 13,000 cycles at 20 A g^{-1}	2 M KOH	Three electrodes	[48]
Silk (cocoon)	Porous and N- doped carbon nanosheets	731	$CaCl_2$	Supercapacitor	34 uF cm^{-2}, 97% after 20 000 cycles at 20 A g^{-1}	6 M KOH	Three electrodes	[49]
Silk (cocoon)	N, O, co-doped hierarchical porous carbon fibers	2643.75	KOH	Supercapacitor	392 F g^{-1} at 1 A g^{-1}	6 M KOH	Three electrodes	[50]
Egg white	N/O/P co-doped 3D hierarchical porous carbon hybrids	2576	$CaCO_3/Na_3PO_4$	Supercapacitor	452 F g^{-1} at 0.5 A g^{-1}, 92.4% retention after 10,000 cycles at 10 A g^{-1}	6 M KOH	Three electrodes	[51]
Soy	3D N-enriched hierarchical porous carbon aerogels	1438	NaCl/NaOH	Supercapacitor	264.3 F g^{-1} at 0.5 A g^{-1}, 98.6% retention after 10,000 cycles	2 M KOH	Three electrodes	[52]
Yeast (bacteria)	Hierarchical mesoporous carbon	997.2	None	Supercapacitor	170 F g^{-1} at 1 A g^{-1}, 84% retention after 10,000 times	6 M KOH	Three electrodes	[53]
Pea (vegetable)	N, O dual-doped porous carbon	3500	KOH	Supercapacitor	413 F g^{-1} at 1.0 A g^{-1}, 92% retention after 20,000 cycles	1 M KOH	Three electrodes	[54]
Silk (sericin)	N-doped hierarchically porous carbons	2723	KOH	Supercapacitor	287 F g^{-1} at 0.5 A g^{-1}, 93% retention after 10,000 times	6 M KOH	Three electrodes	[55]
Soy	Protein-based microporous carbon	1117	KOH	Supercapacitor	336 F g^{-1} at 1 A g^{-1}, 173 F g^{-1} at 10 A g^{-1}	6 mol L^{-1} KOH	Symmetrical	[56]
Zein	N-doped carbon fiber	348.4	None	Supercapacitor	64 μF/ cm2 at 0.5 A g^{-1}, 98% retention after 5000 cycles at 10 A g^{-1}	6 M KOH	Three electrodes	[57]
Zein	Self-Standing hierarchical porous N-doped carbon fibers	1113	CO_2	Supercapacitor	410 F g^{-1} at 1 A g^{-1}, 95% retention after 3000 cycles	6 M KOH	Three electrodes	[58]
Silk (cocoon)	N-doped hierarchically porous carbon	3386	KOH	Supercapacitor	128.8 F g^{-1} at 50 A g^{-1}, 95% reterntion after 4500 cycles at 20 A g^{-1}	1.0 M $TEABF_4$/AN	Symmetrical	[59]
Wheat	Heteroatom doped porous carbon sheets	2724	KOH	Supercapacitor	350 F g^{-1} at 0.5 A g^{-1}	6 M KOH	Three electrodes	[60]
Soy	Heteroatom-doped interconnected porous carbon	2609	KOH	Supercapacitor	405 F g^{-1} at 0.5 A g^{-1}	6 M KOH	Three electrodes	[61]
Soy	N, O co-doped porous carbons	2059	KOH	Supercapacitor	330 F g^{-1} at 0.5 A g^{-1}, (94.6% retention after 10,000 cycles at 2.5 A g^{-1}	3 M KOH	Symmetrical	[62]

(*continued on next page*)

Table 1 (*continued*)

Protein type	Carbon type	SSA ($m^2\ g^{-1}$)	Activation agent	System	Electrochemical performance	Electrolyte	Counter Electrode	Ref.
Egg white	Egg-protein–graphene porous carbons	1365	KOH	Supercapacitor	482 F g^{-1} at 0.1 A g^{-1}, 100% retention after 10,000 cycles 5 A g^{-1}	1 mol L^{-1} H_2SO_4	Pt, Ag/AgCl	[63]
Egg white	Porous carbons	3250	KOH	Li-ion Supercapacitor	172 F g^{-1} (120 mAh g^{-1}) at 0.4 A g^{-1},	1.2 M $LiPF_6$ in EC/DEC/DMC	Si/C	[64]
Silk (cocoon)	N-doped porous carbon	3841	KOH	Supercapacitor	408 F g^{-1} at 0.5 A g^{-1}, 96% retention over 20,000 cycles	6 M KOH	Three electrodes	[65]
Silk (cocoon)	Porous carbon	3050	KOH	Na-ion Supercapacitor	~348 F g^{-1}; 171 mAh g^{-1} at 0.1 A g^{-1}	6 M KOH; 1 M $NaPF_6$ in DEGDME	Na; graphite	[66]
Soy	Porous active carbon	1663.1	KOH	Supercapacitor	337.3 F g^{-1} at 1 A g^{-1}	6 M KOH	Three electrodes	[67]
Soy	N-doped active carbon/ graphene	1412.9	KOH	Supercapacitor	378.9 F g^{-1} at 0.05 A g^{-1}; 93% retention after 10,000 cycles at 2 A g^{-1}	6 M KOH	Three electrodes; symmetrical	[68]
Whey (milk)	N-doped porous carbon	2536	KOH	Supercapacitor	248 F g^{-1} at 0.1 A g^{-1}, 100% retention after 1000 at 5 A g^{-1}	6 M KOH	Symmetrical	[69]
Silk (fibroin)	Graphene/carbon nanocomposites	3200	KOH	Supercapacitor	256 F g^{-1} at 0.5 A g^{-1}, 96.3% retention after 10 000 cycles	6 M KOH	Three electrodes	[70]
Yogurt	N-doped porous carbon	1300	KOH	Supercapacitor	225 F g^{-1} at 2 A g^{-1}; 200 F g^{-1} at 20 A g^{-1}	1 M H_2SO_4; 6 M KOH	Graphite	[71]
Silk	Hierarchical porous N-doped carbon	2494	KOH	Supercapacitor	242 F g^{-1} at 0.1 A g^{-1}	$EMIMBF_4$	Symmetrical	[72]
				Li-ion	261 mA h g^{-1} at 20 A g^{-1}	1 M $LiPF_6$ in EC/DMC	Li	
Silk	Carbon aerogels	180.7	NaOH	Supercapacitor	298 F g^{-1} at 0.75 A g^{-1}	1 M H_2SO_4	Symmetrical	[73]
Egg white	N-rich carbon	805.7	None	Supercapacitor	80 F g^{-1} at 0.25 A g^{-1}	1 M H_2SO_4	Pt, $Hg/HgSO_4$ (with K_2SO_4)	[74]
				Li-ion	716 mA h g^{-1} at 0.1 A g^{-1}	1 M $LiPF_6$ in EC/ DMC	Li	
Silk	Carbon-based microporous nanoplates	30/2557.3	None/KOH	Supercapacitor	264 F g^{-1} at 0.1 A g^{-1}	1 M H_2SO_4	Symmetrical	[27]
Gelatin	N-doped porous carbon	3012	NaOH	Supercapacitor	385 F g^{-1}	6 mol L^{-1} KOH	Symmetrical	[75]
Egg white	N-riched carbon sheets	Not provided	None	Supercapacitor	302 F g^{-1} at 0.5 A g^{-1}; 98% retention after 10,000 cycles	1 M H_2SO_4	Pt; symmetrical	[76]
Amino acids	N/S co-doped hierarchically porous Carbon	900/1109/ 2370/2959	None/NH_4Cl/ KOH/K_2CO_3	Supercapacitor	350 F g^{-1} at 1 A g^{-1}, 100% retention after 5000 cycles at 5 A g^{-1}	6 M KOH	Three electrodes	[77]

Notes: Conventional three electrodes: Pt, Hg/HgO and the Ni foam with the carbon slurry; Symmetrical: both electrodes are the same electrode; EC: ethylene carbonate; DEC: diethyl carbonate; FEC: fluoroethylene carbonate; DMC: dimethyl carbonate; EMC: Ethyl methyl carbonate; DME: dimethoxyethane; DEGDME: diethylene glycol dimethyl ether; TEGDME: tetraethylene glycol dimethyl ether. PVA: polyvinyl alcohol; $TEABF_4$: Tetraethylammonium tetrafluoroborate; AN: acetonitrile; $EMIMBF_4$: 1-Ethyl-3-methylimidazolium tetrafluoroborate. The ratio of electrolyte solvents is 1:1 or 1:1:1.

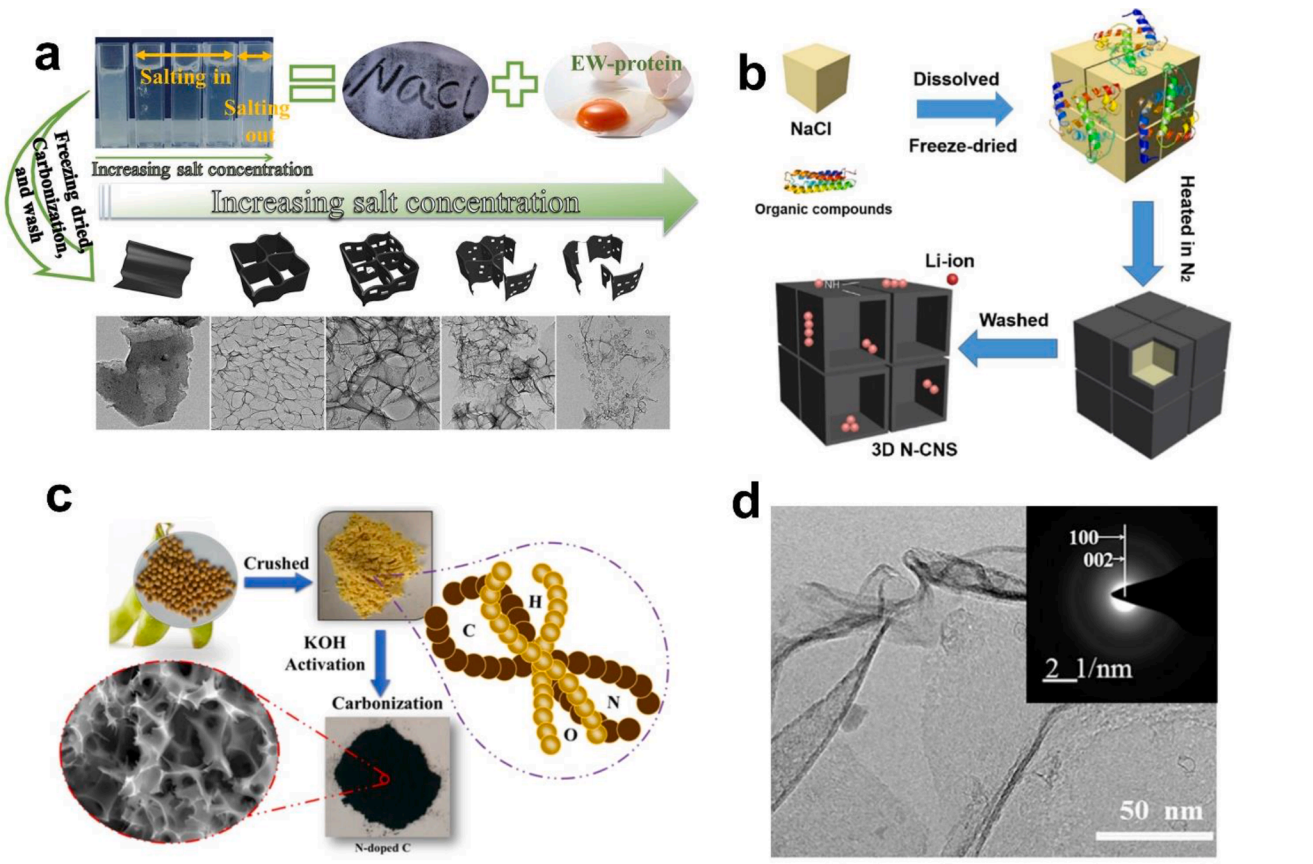

Fig. 2. The protein-derived activated carbons for Li-ion batteries. (**a**) The preparation of hierarchical porous carbon derived from egg white [33]. Reproduced with permission. Copyright 2019, Elsevier. (**b**) The synthesis processes of N-doped carbon nanosheets by soy protein [30]. Copyright 2018, Elsevier. (**c**) The fabrication of porous carbon by using soy protein from soybeans; (**d**) High-resolution transmission electron microscopy (TEM) images of the soy protein-derived carbon calcined at 700 °C [31]. Copyright 2018, Elsevier.

EDS of the carbon fibers demonstrated the unchanged morphology and heteroatoms (N, O)-doping that was originated from the protein polypeptide chains (Fig. 4**b**). The obtained carbon fibers exhibited low ΔE_p values of cathode electrolyte (~ 164.5 mV) and anode electrolyte (~164.6 mV) at a scan rate of 5 mV s^{-1} in VRFBs. In another study, twin cocoon (source of silk protein) was treated by the combination of hydrothermal and carbonization methods (600–1000 °C) to fabricate an N-, O-doped self-standing monolithic carbon, bringing about high electrochemical activity and stability in VRFBs [42]. The pristine twin cocoon composed of silk fibers has poor flexibility due to the presence of sericin (Fig. 4**c**). After degumming process in the boiled alkaline aqueous solution, the cocoon transformed to a high-elastic silk fabric with rich pores (Fig. 4**d**). Thereafter, the black carbonized silk fibers with rich heteroatoms-doping were achieved *via* carbonization process (Fig. 4**e**). The performance enhancements of the resulting carbon in VRFBs were attributed to two aspects of silk protein-derived activated carbons: i) monolithic and interconnected structures increase the electronic/ionic conductivity, flexibility and porosity of electrodes; ii) the defect-rich and N, O-rich surface enhances the activity and reversibility of electrochemical reactions.

2.4. Electrodes of supercapacitors

During the charge/discharge processes of supercapacitors, the electrochemical performance of carbon electrodes is mainly affected by two factors [78]. The first factor is the size distribution of pores that provide ion diffusion channels and a large surface to absorb the charges. The macropores with sizes larger than 50 nm serve as the channels for electrolytes, while the mesopores with smaller sizes of 2–50 nm are the transition pores that increase the ion diffusion rate. The micropores with sizes of less than 2 nm can absorb and store the charges. Therefore, an interconnected carbon structure with appropriate pore size distribution is needed for high-performance supercapacitors. The second factor is the surface chemical constituents that are closely related to the electrode wettability with electrolyte. The surface functional groups or heteroatoms not only provide a quick ion diffusion induced by good wetting, but also produce more active sites for absorbing and storing charges.

Protein molecules possess various quaternary structures and rich heteroatoms (e.g., N, O and S), making them potential raw materials for fabricating heteroatoms-doped porous carbon electrodes with improved performance for supercapacitors. The protein used as the raw materials for carbon electrodes of supercapacitor are plant proteins such as soy (e.g., soybean, soy protein isolate, bean pulps, soy meal, soy flour, etc.), zein, yeast and pea, and animal proteins such as casein (milk colloid), egg protein, silk protein (e.g., silkworm cocoon, fibroin, sericin, etc.), and whey protein.

Soy proteins in various forms and/or using different treatment procedures were used to synthesize heteroatoms co-doped porous carbons for improving the capacitances of supercapacitors in both acidic and alkaline electrolytes [46,48]. For example, an N, O, P, S co-doped porous carbon was prepared by soybean *via* different mass ration of activation agent (KOH) and different carbonization temperatures (500–800 °C), exhibiting an ultra-high capacitance of 685.1 F g^{-1} at 0.5 A g^{-1} in the supercapacitor with the electrolyte of 2 M KOH solution [48]. In addition, by a combination of freeze-drying and carbonization process (Fig. 5**a**), soy protein isolate (a commercial soy product with more than 90% soy protein) was used as the N source to fabricate a N-containing carbon aerogel by the activation agents (NaCl, NaOH [52], KOH) at 600

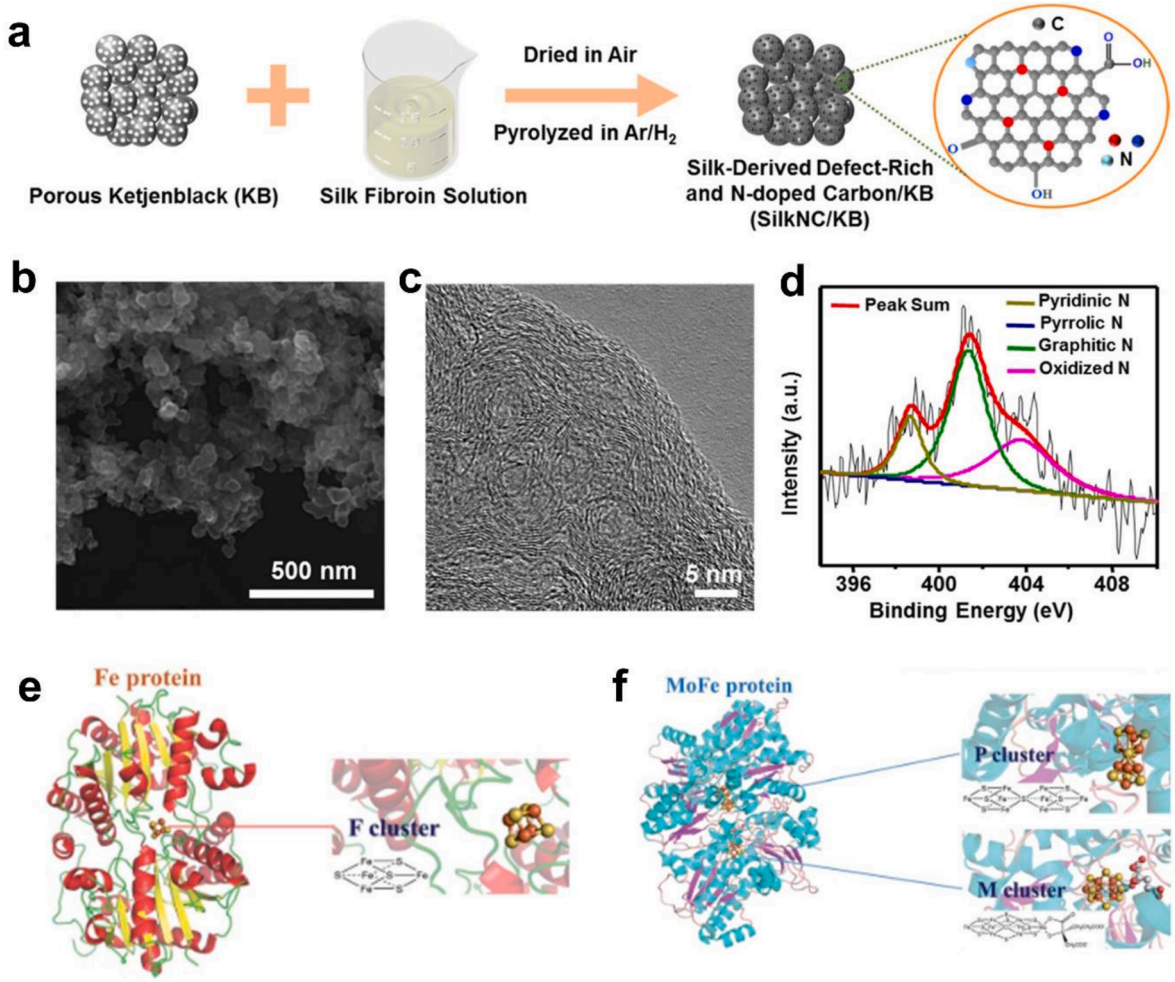

Fig. 3. The protein-derived carbons for the cathode electrocatalysts of metal-air batteries. (**a**) Schematic illustration of preparation process for silk-derived carbon; (**b**) Scanning electron microscopy (SEM) and (**c**) TEM images of silk-derived carbon; (**d**) X-ray photoelectron spectroscopy (XPS) spectrum of N 1s for silk-derived carbon [39]. Copyright 2019, American Chemical Society. (**e, f**) Structural models for the Fe, MoFe protein (soy protein from root nodule) and the corresponding metal clusters in protein architectures [40]. Copyright 2021, Royal Society of Chemistry.

°C [46] and 800 °C [45]. The supercapacitor with the carbon aerogel has specific capacitances of 230–280 F g^{-1} at 0.5 A g^{-1} with 6 M KOH as the electrolyte. Moreover, *via* the activation of different volume concentrations of CO_2 in protection gas (Ar) at 700 °C, soy protein (bean pulps) was carbonized to a controllable porous structure with high SSAs and N-contained functional groups [47,67]. In another studies, different soy protein-products, such as soymeal (a commercial soy product with ~50% soy protein) [62], defatted soy meal, soy flour (with ~50% soy protein) and soy protein isolate, were used to fabricate activated carbons by a time-effective microwave method with ammonium polyphosphate as the additional source of N and P atoms [44]. Among the soy protein-products, soy protein isolate-derived carbon showed a relatively high specific capacitances of 112 F g^{-1} in acidic electrolytes and 94 F g^{-1} in a basic electrolyte. The other soy protein-based material, bean curd stick, treated by a combination process of hydrothermal, freeze-drying and pyrolysis, generated a hollow interconnected structure with a high SSA (2609 m^2 g^{-1}) and O-, N-doping [61]. One more study on applying soy protein as the N source of N-doped carbon/graphene composites for the electrodes of supercapacitors [68].

Casein (milk protein) was employed as the precursor of activated carbon. The casein protein-derived porous carbon with ultra-micropores (< 1 nm) and mesopores/micropores (~2 nm) was synthesized by the protein modulation of graphene oxide sheets [43]. The porous carbon exhibited a high gravimetric capacitance (358.4 F g^{-1}) with an electrolyte (6 M KOH) mass uptake of 10 mg cm^{-2} at 0.1 A g^{-1}. Moreover, with the organic electrolyte composed of ethylene carbonate (EC), ethyl methyl carbonate (EMC) and $LiPF_6$, the supercapacitor with the porous carbon showed a high energy density of 43.0 W h kg^{-1} at the conditions of potential window = 3 V and power density = 300 W kg^{-1}.

Egg protein is an easily available protein in egg white. The heteroatoms co-doped hierarchical porous carbon hybrids were fabricated by Na_3PO_4 denatured egg white and using nano-$CaCO_3$ as the template [51]. The obtained carbon possesses a high SSA (2576 m^2 g^{-1}), more heteroatoms (N, P and O) co-doping and well-balanced pore distribution, delivering a high specific capacitance of 452 F g^{-1} at 0.5 A g^{-1}. In another study, the egg protein-derived carbon *via* using a traditional carbonization/pyrolysis process exhibited energy densities of 257–147 Wh kg^{-1} at power density from 867 to 29,893 W kg^{-1} in Li-ion capacitors [64]. In recent study, with the hydrothermal carbonization process and by using graphene oxide sheets as the template, the egg protein can form a highly porous carbon with a different morphology [63]. Moreover, mesoporous cellular foam silica [74] and perlite [76] were used as templates to synthesize egg white-derived N-enriched carbon (Fig. 5**b**). This carbon showed a continuous integrated macro structure composed of "peanut-like" units, demonstrating its porous morphology (Fig. 5**c**) and exhibiting a specific capacitance of 390 F g^{-1} in supercapacitors.

Silk protein was used to fabricate activated carbon as the active material of supercapacitors. Silkworm cocoon-derived protein was activated by $CaCl_2$ and carbonized at 700 °C to fabricate the activated

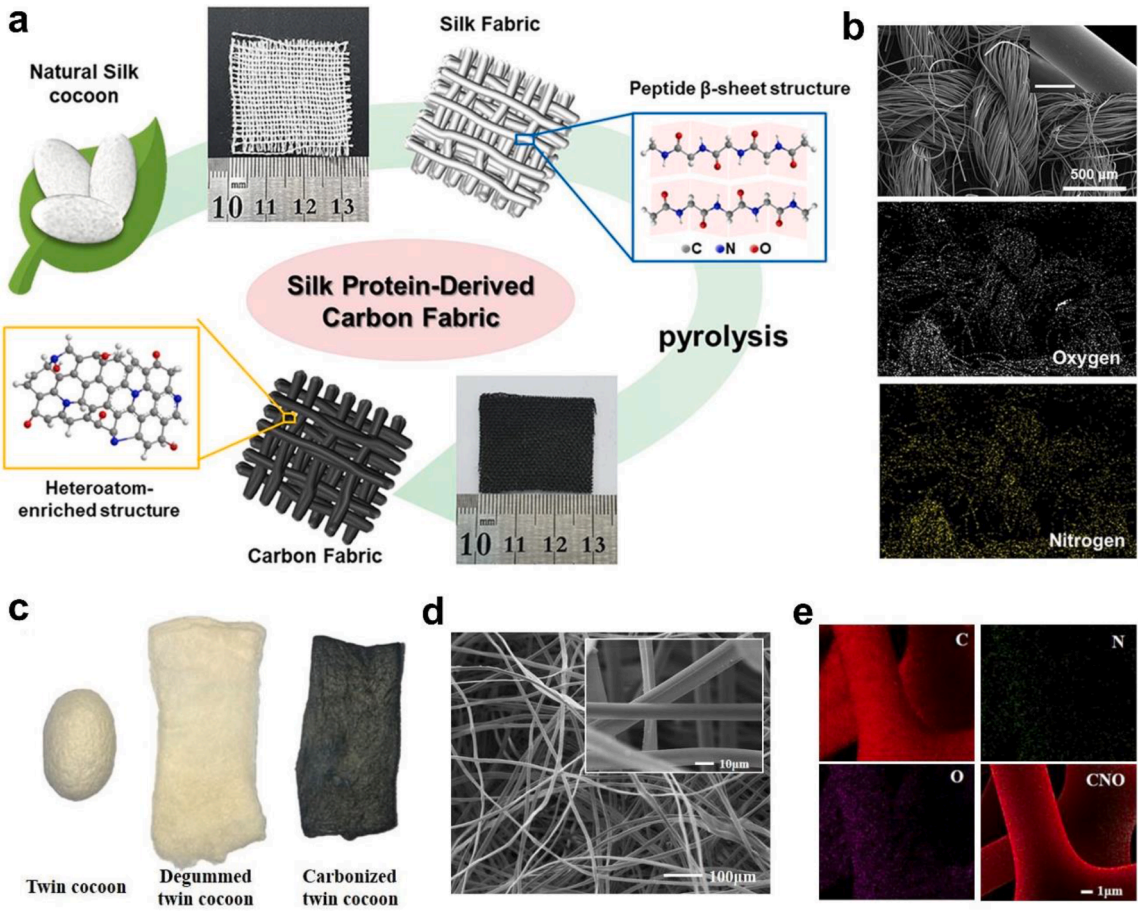

Fig. 4. The protein-derived carbons for the cathode electrocatalysts of redox flow batteries. (**a**) Schematic of the fabrication for silk-derived carbon fibers; (**b**) SEM and energy-dispersive X-ray spectroscopy (EDS) mapping of silk-derived carbon fibers [41]. Copyright 2019, Elsevier. (**c**) The digital images of pristine twin cocoon, hydrothermal treated twin cocoon and carbonized twin cocoon; (**d**) SEM images of the pristine twin cocoon; (**e**) EDS elemental mapping of the carbonized silk fibers [42]. Copyright 2021, Elsevier.

carbon with protuberant porous nanosheets possessing a high SSA (731 $m^2\ g^{-1}$), high N-doping content (7.91 atomic%) and wide pore size distribution (0.5–65 nm) [49]. This activated carbon showed a high areal capacitance of 34 F cm^{-2} at 20 A g^{-1} in supercapacitors with 6 M KOH as electrolyte. Similarly, cocoons was pyrolyzed to hierarchical porous N-rich ultrathin layer assembled carbon fibric *via* the activation of different amounts of KOH at 800 °C and the modulation of N contention by g-C_3N_4 [50,59,65,72]. The carbon fibers possess an extremely high SSA of 2643.75 $m^2\ g^{-1}$, hierarchical pores and high N-doping of 6.05%, leading to a high specific capacitance of 392 F g^{-1} at 1 A g^{-1} in the supercapacitor with 6 M KOH as electrolyte. In addition, one of the two main proteins of cocoons, sericin, was carbonized and activated by KOH at 800 °C, forming a N-doped hierarchically porous carbon with a high SSA of 2723 $m^2\ g^{-1}$. This carbon exhibited a specific capacitance of 287 F g^{-1} at 0.5 A g^{-1} in supercapacitors [55]. The other main cocoon protein, fibroin, was employed as the precursor to synthesize activated carbon by a facile one-step carbonization/pyrolysis process [27,66]. This carbon material has lateral sizes greater than 5 μm and the thickness is less than 100 nm (Fig. 5**d, e**). Furthermore, the fibroin-derived carbon has a high SSA (~3050 $m^2\ g^{-1}$) and rich O (17.4 wt%), N (2.9 wt%)-doping, leading to a high specific power of ~1900 W kg^{-1} at ~77 Wh kg^{-1} in Na-ion supercapacitors. With the incorporation of graphene, the fibroin-derived carbon has a larger SSA of 3200 $m^2\ g^{-1}$ and a specific capacitance of 256 F g^{-1} at 0.5 A g^{-1} in supercapacitors [70]. Moreover, a carbon aerogel fabricated by fibroin and graphene oxide was demonstrated to have a rough surface morphology, electroactive N configurations and O, N-doping, resulting in good wetting with electrolyte in supercapacitors [73].

Zein, corn protein, is the by-product of corn starch processing and one of the main products of bioethanol production. In the application of supercapacitors, zein-lignin carbon fabric electrode was prepared by electrospinning and carbonization [58]. The thickness and pore size (< 50 nm) of the carbon fabric was modulated by changing the lignin content from 0 to 50%. The optimized carbon fibers exhibited a high specific capacitance of 410 F g^{-1} at 1 A g^{-1} in the supercapacitor with 6 M KOH as electrolyte. With the incorporation of Ca^{2+} in the electrospinning process, zein fibrous structure was well maintained during the carbonization process by the calcium oxide [57]. The resulting carbon possesses a high N contention (7.5%) and interconnected fibrous network with abundant *meso*/micropores on the surface of fabric.

Gelatin is an animal derivative protein. With the carbonization (at 450 °C) and activation of various amounts of NaOH at 600 °C, the resulting gelatin-derived carbon has a high SSA (3012 $m^2\ g^{-1}$) and high N content (9.26 at%) [75]. Wheat gluten is a by-product of flour production that contains 70% protein. The wheat gluten-derived carbon activated by KOH at different temperatures (600–800 °C) showed a synergetic effect of pore size and heteroatoms-doping on the performance of supercapacitors [60]. In addition, a protein-rich yogurt-derived carbon possesses a very high N contention (12 wt%) even under the pyrolysis temperature of 800 °C [71].

Other proteins, such as those from yeast, pea, and whey, used to fabricate carbon electrodes for supercapacitors were also reported. Yeast protein was used as the raw materials of the hierarchical mesoporous carbon. The Yeast protein-derived carbon was fabricated by carbonizing

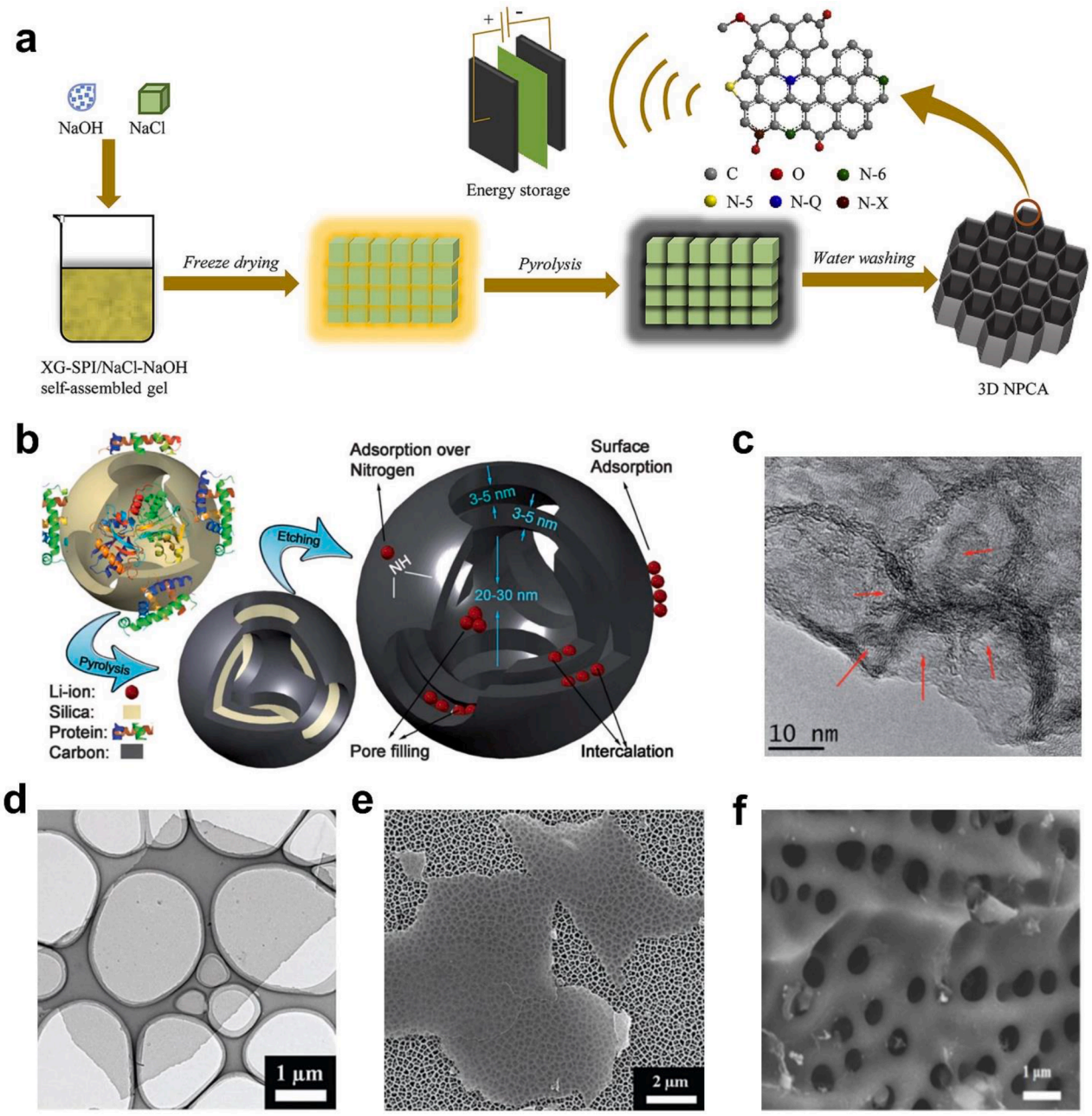

Fig. 5. The protein-derived carbons for the electrodes of supercapacitors. (**a**) The fabrication process of 3D N-enriched hierarchical porous carbon aerogel from soy protein [52]. Copyright 2020, Elsevier. (**b**) The egg protein-derived mesoporous carbon is synthesized in the pores of mesoporous cellular foam and the proposed Li storage mechanism; (**c**) TEM images of egg protein-derived carbon pyrolyzed as 850 °C [74]. Copyright 2013, Royal Society of Chemistry. (**d**) Field-emission transmission electron microscope (FE-TEM) image of the silk-derived microporous carbon nanoplates containing numerous heteroatoms on a holey carbon grid; (**e**) FE-SEM image of the silk-derived carbon film on Al_2O_3 template [27]. Copyright 2013, Wiley-VCH. (**f**) The SEM images of amino acid (Lys)-derived carbon [77]; Copyright 2019, American Chemical Society.

the yeast protein-enriched waste diatomite obtained from the beer filtration process [53]. The diatomite was applied as the template for building the mesoporous structure. Moreover, high-performance pea protein-derived carbon was synthesized by optimizing the amount of KOH and pea protein to 1:4 and pyrolysis temperatures at 800 °C [54]. The carbon possesses a high SSA (3500 $m^2\ g^{-1}$) and pore volume (1.76 $cm^3\ g^{-1}$), building a very high specific capacitance of 413 F g^{-1} at 1.0 A g^{-1} in 1 M KOH electrolyte. In addition, with the catalytic graphitization of Ni atom during pyrolysis at 700 °C, whey protein was used to fabricate a N-doped carbon with high specific surface area and high porosity, resulting in a high capacitance of supercapacitors [69].

In addition to protein, some amino acids of protein were also applied as the precursor of activated carbon. The amino acid protic ionic liquids [79] composed of H_2SO_4 and different amino acids (e.g., Lys, Trp-and Phe) were directly carbonized and activated at 900 °C by various agents (e.g., NH_4Cl, KOH, and K_2CO_3). Among the obtained carbons, the K_2CO_3-activated Lys-derived carbon exhibited rich micropores and mesopores (Fig. 5**f**) that provide rapid ion transport in supercapacitors [77].

2.5. Summary

Various natural proteins were applied as the raw materials of activated carbon for electrodes of EESDs. Based on physicochemical

properties of proteins, the activated carbons with different dimensions (including 1D, 2D, and 3D) of porous structures and high N-doping content were obtained. (1) 1D: carbon microrods, nanotubes and microfibers were prepared *via* carbonizing silk proteins (e.g. fibroin, pyroprotein and sericin) and electrospinning protein fibers (e.g., zein). (2) 2D: carbon sheets were fabricated by denaturation of proteins and carbonation of the denatured proteins (e.g., soy, silk, egg white protein, etc.). (3) 3D: interconnected porous bulk carbons were synthesized by the activation of carbonized protein (e.g., soy, silk, wheat, milk protein, etc.) during their pyrolysis process. These protein-derived carbons possessed rich hierarchal pores that facilitated the electrolyte flow and ion transfer in electrodes. Moreover, the large SSAs and rich heteroatoms-doping of protein-derived carbons induced abundant active sites for ion storage or chemical reactions. Therefore, the electrodes with protein-derived carbons built high-performance EESDs such as Li-, Na-, K-ion batteries, Li-, Zn-air batteries, VRFBs and supercapacitors.

3. Protein-modified active materials

Proteins have abundant polar functional groups (e.g., -COO^-, -NH_3^+, -OH, C═O) that can build strong interactions with ions and inorganic particles. Based on the unique characteristics of protein, inorganic particles were modified with different structures (e.g., core-shell, nanosheet, 3D composites, etc.) by using protein were obtained *via* (1) the formation of inorganic nanoclusters at the binding sites of protein and (2) absorption of protein molecules on the surface of inorganic particles. Most inorganic active materials (e.g., Si, transition metal chemicals, etc.) were modified by proteins to improve their electrochemical performance in EESDs. The performance of various protein-modified active materials for electrodes of EESDs is summarized in Table 2.

3.1. Electrodes of Li-, Na-ion and Li–metal batteries

The challenges of high-performance active materials for batteries originate from the poor electrical/ionic conductivity, big volume deformation and/or the serious dissolution of active materials in

Table 2
Protein-modified active materials for electrodes of EESDs.

Protein	Electrode	Systems	Electrochemical performance	Electrolyte	Counter Electrode	Ref.
Wheat	Hierarchical porous Si /N-doped carbon composite	Li–ion	696.1 mAh g^{-1} over 300 cycles at 1 A g^{-1}	1 M $LiPF_6$ in EC/DEC/EMC+ 5 wt% FEC	Li	[80]
Soy (tofu)	Si@N-doped activated carbon	Li–ion	731.6 mA h g^{-1} after 300 cycles at 1 A g^{-1}	1 M $LiPF_6$ in EC/DEC/EMC+ 5 wt% FEC	Li	[81]
Collagen	γ-MnO_2 mesocrystals	Li–ion	1614.7 mA h g^{-1} at 0.2 C of 1st cycle	1 M $LiPF_6$ in EC/DEC	Li	[82]
Kelp	N-containing MnO/C hybrid	Li–ion	978 mAh g^{-1} at 0.2 A g^{-1}	1 M $LiPF_6$ in DMC/EMC/EC	Li	[83]
Egg white	$LiFePO_4$@C	Li–ion	120 mA h g^{-1} at 5 C	1 M $LiPF_6$ in EC/DMC	Li	[84]
Eggshell membrane	α-$Ni(OH)_2$ nanowires formed on eggshell membrane	Li–ion	827 mAh g^{-1} after 10 cycles at 100 mA g^{-1}	1 M $LiPF_6$ in EC/DEC	Li	[85]
Vegetable	$Li_3V_2(PO_4)_3$@C	Li–ion	100 mAh g^{-1} at 15 C	1 M $LiPF_6$ in EC/DMC	Li	[86]
Collagen	Hierarchically C@SnO_2@C nanofiber bundle	Li–ion	430mAh g^{-1} at 1.0 A g^{-1}	1 M $LiPF_6$ in EC/EMC/DMC	Li	[87]
BSA	C-coated SnO_2 nanocrystal	Li–ion	648 mAh g^{-1} after 100 cycles at 100 mA g^{-1}	1 M $LiPF_6$ in EC/DEC	Li	[88]
Silk (fibroin)	S@C	Li–S	815 mA h g^{-1} after 60 cycles at 0.2 C	1 M LiTFSI in DOL/DME	Li	[89]
Pomegranate	S@hierarchical porous carbon	Li–S	550 mAh g^{-1} after 500 cycles at 0.1C	Not indicated	Li	[90]
Soy	S@O- and N- rich hierarchical porous carbon nanostructure	Li–S	950 mA h g^{-1} at 0.2C	1 M LiTFSI in DOL/DME + 2 wt% $LiNO_3$	Li	[91]
Spirulina	C/S composite	Li–S	1670 mA g^{-1} after 100 cycles at 1 C	1 M LiTFSI in DOL/DME + 1 wt% $LiNO_3$	Li	[92]
Hemoglobin (blood)	Fe/C composite microfiber catalyst	Li–air	2231 mAh g^{-1} at 100 mA g^{-1} (2.3–4.5 V)	1 M LiTFSI in DEGDME	Li	[93]
Elastin	Transition metal-N-C (M-N/C) catalysts	Li–air	12 441 mAh g^{-1} at 100 mA g^{-1} (2–4.25 V)	1 M $LiCF_3SO_3$ in TEGDME	Li	[94]
Soy	Pt/RuO_2-decorated mesoporous N-doped carbon	Li–air	5724.1 mA h g^{-1} at 100 mA g^{-1}	1 M LiTFSI in TEGDME	Li	[19]
BSA	SnSe-thermal-treated protein@rGO	Na–ion	503.9 mAh g^{-1} after 100 cycles at 0.1 A g^{-1}	1 M $NaClO_4$ EC/PC	Na	[95]
Squid ink	3D TiO_2 hollow spheres (mesocrystal)	Na–ion	110 mA h g^{-1} after 1000 cycles at 1 A g^{-1}	1 M $NaClO_4$ in EC/DEC	Na	[96]
Pig blood	2D Zn-Fe single-atom porous carbon catalyst	Zn–air Fuel cells (AEMFCs)	220 mW cm^{-2} 352 mW cm^{-2}	6.0 M KOH H_2/O_2	Zn Symmetrical gas diffusion layer	[97]
BSA	Protein-coated MoS2/Gr nanosheet	Zn–air	130 W h kg^{-1}, OCV = 1.4 V	4 M KOH	Zn	[98]
Soy	NiFe-LDH nanowalls anchored on Fe-N-C matrix	Zn–air	OER ($E_{j=10}$ = 1.53 V vs. RHE) and ORR ($E_{1/2}$ = 0.91 V vs. RHE)	6.0 M KOH + 0.2 M ZnAC	Zn	[18]
Silk (fibroin)	Microporous carbon nanoplate/RuO_2	Super-capacitor	458 F g^{-1} after 1000 cycles	0.5 M H_2SO_4 electrolyte	Pt, Ag/AgCl	[99]
BSA	CoS_2 nanodots anchored heteroatom-doped carbon layer	Supercapacitor	565 F g^{-1} at 1 A g^{-1}, ~100% retention after 10, 000 cycles at 2 A g^{-1}	6.0 M KOH	Three-electrode	[100]
Hemoglobin (blood)	Hemeprotein-Ni	Supercapacitor	2052 F g^{-1} at 0.4 mA	6 M NaOH	Three-electrode	[101, 102]

Notes: BSA: Bovine serum albumin; PP: polypropylene; PE: polyethylene; PVA: poly(vinyl alcohol); EC: ethylene carbonate; DEC: diethyl carbonate; PC: propylene carbonate; FEC: fluoroethylene carbonate; DMC: dimethyl carbonate; EMC: Ethyl methyl carbonate; DOL: dioxolane; DME: dimethoxyethane; AEMFCs: Anion Exchange Membrane Fuel Cells; Gr: Graphene; OCV: Open circuit potential; NiFe-LDH: NiFe layered double hydroxide. OER: oxygen evolution reaction, RHE: reversible hydrogen electrode; ORR: oxygen reduction reaction; DEGDME: diethylene glycol dimethyl ether; TEGDME: tetraethylene glycol dimethyl ether.

electrolytes. The resultant large resistance, severe active material pulverization and the loss of active materials (e.g., dissolution of polysulfide and Mn cation in electrolytes) cause the poor performance of batteries. To solve these issues, reducing the particle sizes of active materials to the nano scale is a widely studied method to obtain a short electron transport distance, large SSA of active materials and small volume expansion during the Li^+/Na^+ insertion/desertion processes. Among various efforts of modifying the structures of active materials by using protein, more studies were on building pure active materials with unique nanostructures such as nanospheres, nanosheets, 3D porous structures, etc. Other reported work was on creating nanocomposites with designed structures such as core@shell and active material nanoparticles-incorporated matrices.

The proteins such as wheat protein, soy protein, bovine serum albumin (BSA, protein from animal blood), collagen, egg white, vegetable protein, fibroin (silk) and soy protein were reported on assisting the formation of active materials.

3.1.1. *Si and alloy anodes in Li- and Na-ion batteries*

Si is a highly recognized promising active material for anodes of high-energy-density Li-ion batteries as its specific capacity (4200 mA h g^{-1}) is over ten times of the commercial graphite anode. However, the

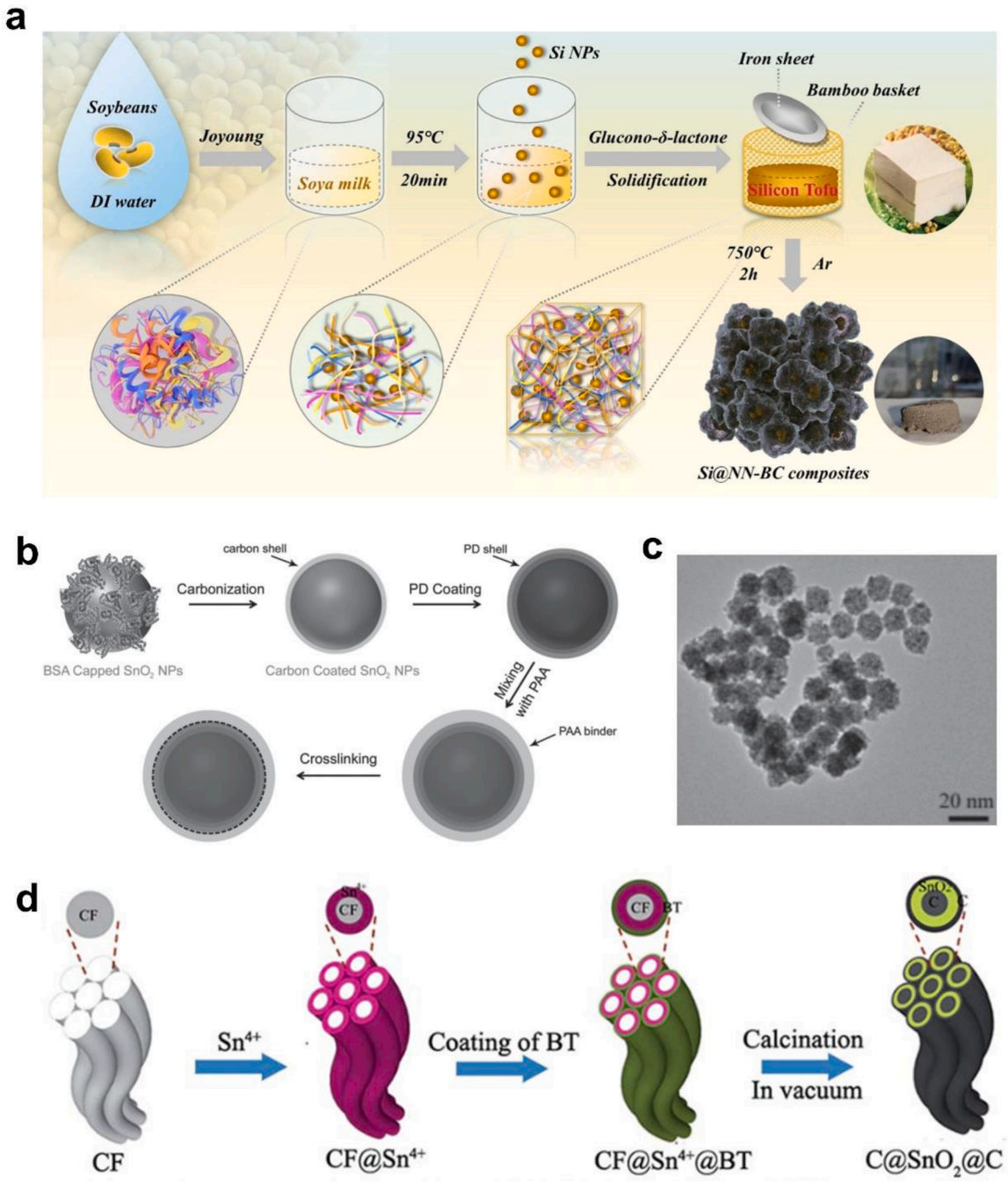

Fig. 6. Protein-modified active materials for Li-ion batteries. (a) Fabrication of the Si@natural N-doped activated carbon composites derived from Si/tofu (soy protein) precursor [81]. Copyright 2021, American Chemical Society. (b) The formation of polydopamine (PD) buffered protein (BSA)-derived carbon-coated SnO_2 nanocrystals and crosslink reaction between PD buffer and polyacrylic acid (PAA) binder; (c) TEM images of bovine serum albumin (BSA)-capped SnO_2 nanoparticles [88]. Copyright 2014, Wiley-VCH. (d) The preparation procedures of the collagen fiber (CF)-derived C@SnO_2@C nanofiber bundle [87]. Copyright 2016, Royal Society of Chemistry.

dramatic volume change (~400%) of the Si anode during the insertion/desertion processes of Li^+ causes poor cycling stability of the battery electrodes, due to the electrode pulverization, unstable solid electrolyte interphase (SEI) formation and poor electrical conductivity. Thus, building a shell or a confined structure with good mechanical performances (high elasticity) and high ionic/electronic conductivities for Si nanoparticles is an effective strategy to alleviate the impact of volume expansion [7,103].

Decorating Si nanoparticles with a carbon layer is a facile and cost-effective strategy to mitigate the volume expansion and improve electrical conductivity. For example, the mixture of protein-containing wheat flour and Si nanoparticles was fermented by the yeast, constructing a unique hierarchical porous carbon matrix for Si particles after carbonization [80]. With the doping of N atoms derived from protein, the porous Si/C composites achieved a stable specific discharge capacity of 696.1 mAh g^{-1} for over 300 cycles at a current density of 1 A g^{-1}. In addition, a Si/C was prepared by using soy protein as the carbon source [81]. The soy milk made from soybean was mixed with Si nanoparticles and glucono-δ-lactone, forming a Si tofu gel after a solidification process. Followed by freeze-drying and carbonization processes, a core–shell structure of Si@N-doped porous carbon was synthesized (Fig. 6**a**). Within Li-ion batteries, this Si@C composite exhibited a stable cycling performance with a specific capacity of 731.6 mAh g^{-1} after 300 cycles at a high rate of 1 A g^{-1}. Their electrochemical performance improvement was attributed to the synergistic effect of the porous structure and N-doping in the composite.

With combination processes of protein (BSA)-directed self-assembly, low-cost vacuum filtration and the followed low-temperature annealing, a self-supporting electrode of carbon-coated tin selenide (SnSe) nanosheets was obtained [95]. The hierarchical 3D framework of this composite was found with a good dispersion of SnSe nanosheets, which were well-confined in the interconnected reduced graphene oxide and BSA-derived carbon network. As an anode electrode for Na-ion batteries, this composite showed a stable specific capacity of 503.9 mAh g^{-1} at 0.1 A g^{-1} after 100 cycles.

3.1.2. Transitional metal oxide anodes for Li- and Na-ion batteries

Transitional metal oxides (e.g., Fe_2O_3 and SnO_2) are potential anode materials for batteries because of their high specific capacities, low cost and natural abundance [8–11]. The Li storage mechanism of transitional metal oxides are based on their conversion reactions. When as the anodes, similar to that of Si, transitional metal oxides are also plagued by poor intrinsic conductivity and volume expansion during the cycling process. To solve these issues, some animal proteins, such as BSA (protein from animal blood), collagen (protein fiber from cattle skin), and eggshell (primarily composed of fibrous protein such as collagen) were reported on the modification of active materials for Li- and Na-ion batteries.

A BSA-capped SnO_2 was prepared as carbonization precursor of composite nanospheres SnO_2@C [88]. To build a good buffer layer between SnO_2@C and polyacrylic acid (PAA) binder, a polydopamine (PD) with controlled thickness was coated on the SnO_2@C. The BSA capped SnO_2@C nanocrystals formed a robust network in the anode electrode *via* the crosslink reaction between the buffer layer and binder (Fig. 6**b, c**). As a result, the obtained electrode presented an enhanced reversible specific capacity of 648 mAh g^{-1} at a current density of 0.1 mA g^{-1} after 100 cycles.

In a recent study, collagen (protein fiber from cattle skin) was used as the carbon source and template for synthesizing a sandwich-structured carbon nanofiber@SnO_2@carbon coating (C@SnO_2@C) nanofiber bundle (Fig. 6**d**) [87]. The material C@SnO_2@C was synthesized by a combination of hydrothermal and calcination (500 °C for 2 h) processes, exhibiting enhanced rate performance and cycling stability when used as the anode for Li-ion batteries. This performance enhancement was due to the efficient ambi-polar diffusion kinetics and the volume change buffer function of C@SnO_2@C architecture.

In addition, a NiO—Ni incorporated carbon was synthesized by a formation of a-$Ni(OH)_2$ nanowires in the pores of eggshell membrane (primarily composed of fibrous protein such as collagen) and calcination of the precursor at 300 °C [85]. The presence of Ni metal in NiO nanoparticles is due to the reduction of eggshell membrane on Ni^{2+}. At a current density of 0.2 A g^{-1}, the NiO—Ni/C composites build a specific capacity of 750 mAh g^{-1}, which is much higher than that of NiO (350 mAh g^{-1}).

In another study, a unique mesocrystal TiO_2 hollow sphere structure composed of TiO_2 nanoparticles was rationally prepared by using protein-rich sulfonated-squid ink as templates [96]. The squid ink comprised large amounts of nanosphere particles with diameters of ~100 nm. Each nanosphere particle was composed of a protein/polysaccharide composite shell and a melanin core. With the formation and growth of TiO_2 grain on ink nanospheres, and followed by a heating process in the air to remove the carbon core, the mesocrystal TiO_2 hollow spheres with a shell thickness of 20–30 nm were obtained. When employed as the anode for Na-ion batteries with an ether-based electrolyte, the TiO_2 spheres exhibited superior cycling stability of 110 mA h g^{-1} after 1000 cycles at 1 A g^{-1}.

3.1.3. Cathodes for Li-ion batteries and Li–metal batteries

Low electric conductivity and low ionic diffusion rate are the two major issues for cathode materials. To solve these issues, various nanostructures of active material/carbon composites for the cathode of Li-ion batteries were synthesized by protein precursors. For example, $LiFePO_4$ nanoparticles were homogenously mixed with liquid egg white, and then were sintered into a N-doped carbon-coated $LiFePO_4$ [84]. The resulting composite cathode showed a specific capacity of 144 mA h g^{-1} at 1 C, which was believed to be due to the facilitated ion transportation and enhanced electric conductivity in electrodes. In another study, a vegetable protein was applied as the carbon coating shell for $Li_3V_2(PO_4)_3$ *via* sintering the gel-state protein/$Li_3V_2(PO_4)_3$ mixture at 350 °C for 5 h and then pyrolyzed at 750 °C for 10 h [86]. The resulting $Li_3V_2(PO_4)_3$@C composite exhibited a high specific capacity of 100 mAh g^{-1} at a high rate of 15 C in the voltage range of 3.0–4.3 V.

Li-S batteries are an important type of Li-metal batteries, and are recognized as one of the promising future energy storage devices due to their high theoretical energy density of 2600 Wh kg^{-1} and the low cost of S with high natural abundance. However, the S cathode suffers from its low electronic/ionic conductivities, dissolution of the intermediate products (Li_2S_x, $4 \leq x \leq 8$) in electrolyte, and a huge volume expansion during the cycling process, resulting in a poor cycling performance of Li–S batteries. To solve these issues, numerous S/C composites were prepared to immobilize S, improve the electric/ionic conductivities of the S electrode and possess a large SSA. Moreover, the porous carbon can absorb Li_2S_x that are dissolved in the electrolyte, thus, improving the utilization of S and reducing the shuttle effect of Li_2S_x. The proteins (e.g., silk protein, soy protein) derived porous carbon were employed as the host for S electrodes [89–92]. For example, the silk fibroin-derived carbon was prepared *via* freeze-drying and carbonization processes [89]. The S/C composite was synthesized by heating the obtained porous carbon with a sulfur mixture in an argon-filled autoclave at 155 °C for 12 h. The resulting electrode exhibited a reversible capacity of 815 mA h g^{-1} at 0.2 C after 60 cycles. In a recent study, soybean was used to synthesize a N, O-doped hierarchical porous carbon by a combination process of hydrothermal and pyrolysis. The resulting carbon was mixed with S powder and then heated at 155 °C for 12 h in a sealed autoclave for fabricating the S/C composites [91]. With a S loading of 5.5 mg cm^{-2} and 80% S contents, the Li-S battery displayed a specific capacity of 950 mA h g^{-1} at 0.5 C.

3.2. Cathode electrocatalysts for metal–air batteries

3.2.1. Li–air batteries

Li–air batteries have a high energy density of ~3500 W h kg^{-1} while

suffer from high overpotentials and poor cycling performance. These problems are caused by the formation and accumulation of Li_2O_2 on the air-electrode, which deteriorates the charge transfer capacity and the catalytic activity of electrodes. The formation of Li_2O_2 is during the discharge process of the ORR, which is $2Li + O_2 + 2e^- \rightarrow Li_2O_2$, the OER during the charging process is $Li_2O_2 \rightarrow 2Li + O_2 + 2e^-$. To accommodate the accumulation of Li_2O_2 on the air-electrode and reduce the over-potential during the charging process, various carbon materials including those modified by proteins were used as the hosts for catalyst nanoparticles, making the accommodation of Li_2O_2 on cathode and high electrical conductivity.

Thus far, soy protein and blood protein-derived porous carbon as the host for incorporating dispersed catalyst particles was demonstrated to be a promising method to improve their electrochemical performance due to the multifunctionality and renewable properties of proteins. For example, tofu, soy protein, was used as the raw material of carbon host for Pt and RuO_2 catalyst [19]. Tofu was dried, carbonized and activated by KOH to form a N-doped carbon host, thereafter, a RuO_2/C composite was synthesized by the growth of RuO_2 in the carbon host, followed by a reduction process to decorate RuO_2/C composite with Pt nanoparticles. The resulting Pt/RuO_2@C composite had a good dispersion of Pt/RuO_2 electrocatalysts in the porous carbon host, leading to a high-performance Li–air battery with a high specific capacity of 5724.1 mA h g^{-1} at 0.1 mA g^{-1} and a low voltage gap of 0.64 V at 2 A g^{-1}.

In another study, hemoglobin from bovine blood was employed to fabricate Fe/C composite microfiber by the combination of electro-spinning, carbonization (250 °C for 1 h under O_2 atmosphere) and reduction (650 °C for 2 h under H_2/Ar atmosphere) processes (Fig. 7**a**) [93]. The as-spun hemoglobin microfibers (Fig. 7**b**) and the prepared Fe/C microfibers after calcination (Fig. 7**b**) both showed a uniform and flattened morphology. In Li–air batteries, the Fe/C microfiber catalyst showed an improved CE of 100% compared to that of 76% for the conventional carbon catalyst. Moreover, the charge voltage of the Fe/C-contained cell decreased, which was attributed to the high

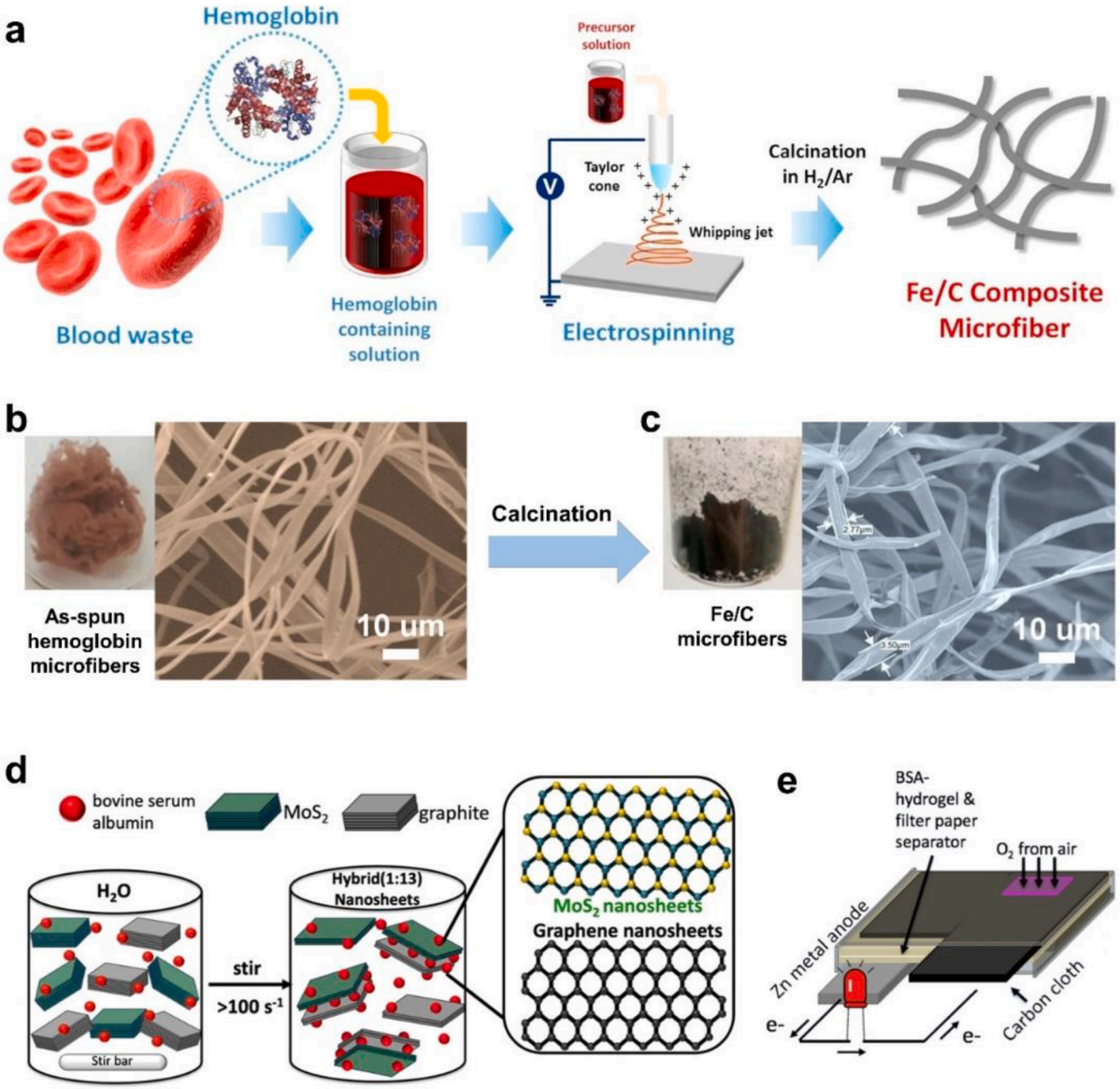

Fig. 7. Protein-modified active materials for metal-air batteries. (**a**) Schematic illustration of the synthetic procedure of Fe/C microfibers from hemoglobin using electrospinning and calcination under a reducing atmosphere; (**b**) As-spun hemoglobin microfibers obtained by the electrospinning method; (**c**) Fe/C microfibers obtained by a two-step calcination of the as-spun microfibers [93]. Copyright 2019, Elsevier. (**d**) Simply-stir production of hybrid MoS_2/Gr nanosheets on a benchtop reactor (top left) assisted by BSA (red spheres); (**e**) A schematic depiction of a Zn−air battery consisting of a protein-nanosheet hydrogel separator [98]. Copyright 2021, American Chemical Society.

catalytic activity of Fe/C microfibers.

3.2.2. Zn–air batteries

Zn–air batteries have a high theoretical specific energy density of 1218 Wh·kg^{-1} and possess advantages of good safety, low cost, and environmental friendliness. Therefore, Zn–air batteries are a good alternative to the EESDs needed in power plants. However, even though the primary Zn–air batteries have been widely applied in navigation light and hearing aids, the secondary Zn–air batteries are heavily plagued by their poor cycle performance. One of the major reasons causing the short lifespan of Zn–air batteries is the corrosion and structural change of cathode electrocatalysts during cycling. The electrocatalysts may be corroded at a high current level in alkaline electrolytes and lose the electrocatalytic activity. The structural change of Zn cathode can destroy gas diffusion layers, inducing the formation of oxygen bubbles in the cathode that impedes contact between electrolyte and electrocatalyst. Moreover, the agglomeration of electrocatalyst particles formed during cycling reduces their electrocatalytic activity and increases the electric resistance. Based on these issues, building the cathode structure with a highly dispersed electrocatalyst, rich pores and high electric conductivity is an attractive strategy to prolong the lifespan of Zn–air batteries.

As mentioned above, proteins with rich functional groups and ion interactions are important precursors or templates for high-performance electrodes. The reported proteins on modifying active materials of Zn–air batteries include soy protein, hemoglobin, and BSA, etc.

Metal ions have strong interactions with proteins, forming highly dispersed metal-hydrolysates in the precursor solutions. A Fe–N–C matrix derived from soy protein was employed as the host for supporting the vertically anchored ultrathin NiFe nanosheet [18]. The Fe–N–C was prepared by a solid carbonization method with the precursor mixture of soybean and $FeCl_3{\cdot}6H_2O$. Then, during the conventional coprecipitation method for NiFe nanosheet preparation, the resulting Fe–N–C was added to the solution to serve as the matrix for the nucleation and growth of NiFe nanosheets. This Fe–N–C exhibited a robust electrocatalytic activity of OER ($E_{j=10} = 1.53$ V vs. RHE) and ORR ($E_{1/2} = 0.91$ V vs. RHE), and presented high stability of cycling performance in Zn-air batteries. Recently, pig blood containing abundant proteins (e.g., hemoglobin) was applied to fabricate an electrocatalyst with a high dispersion of Fe single-atom sites and a 2D sheet-like porous structure [97]. Various amounts of zinc nitrate were added into the protein-rich precursor solution as the activation agents for the carbon materials. After hydrothermal and pyrolysis processes (900–1000 °C), a porous structure with rich even-distributed Fe–N–C sites was generated. The resulting Zn-incorporated Fe single-atom porous carbon catalyst showed a power density of 220 mW cm^{-2} in Zn–air batteries.

A facile one-pot and top-down method assisted by BSA protein was developed to fabricate MoS_2/graphene hybrid nanoplatelets with high productivity in aqueous solutions [98]. BSA was employed as the exfoliant and dispersal agent to generate large amounts of the hybrid suspensions rapidly. The phenyl and disulfide groups of BSA have a binding energy of 0.51 eV with MoS_2, which is much larger than the binding energy among adjacent MoS_2 layers (0.21 eV) (Fig. 7**d**). In Zn–air batteries as show in Fig. 7**e**, the MoS_2/graphene composite with a component mole ratio of 1:13 presented improved ORR activities, high open-circuit voltages of 1.4 V and superior specific energy density of ~130 W h kg^{-1}.

3.3. Electrodes of supercapacitors

The electrodes-active materials for pseudocapacitaor (one type of supercapacitors) are usually composed of transition metal oxides (e.g., CoS_2, RuO_2, MnO_2, NiO, Fe_2O_3, etc.) and a conductive matrix (e.g., carbon, polypyrrole, or polyaniline, etc.). To increase the electric conductivity and ion absorption capacity of active materials, various protein-modified structures were reported. The reported proteins for modifying active materials of pseudocapacitor include BSA, hemoglobin, myoglobin and cytochromes, which are all from body fluids with strong metal–ion interactions.

Using BSA as the template and conductive matrix for CoS_2, a CoS_2 nanodots-anchored carbon composite was prepared by a hydrothermal process at 200 °C for 10 h [101]. The composite nanoparticles were composed of highly dispersed anchored crystalline CoS_2 nanodots in the carbon structure and the protein-derived carbon layer with heteroatoms (e.g., N and S) doping. The resulting CoS_2@C composite was fabricated *via* a facile low-temperature hydrothermal process. Compared to other studies, this method avoids using high-temperature annealing procedures that are energy-consuming in conventional activated carbon preparation processes. The CoS_2@C composite not only built a specific capacitance of 565 F g^{-1} (vs. 176 F g^{-1} of CoS_2) at the current density of 1 A g^{-1} in supercapacitors, but also exhibited a low overpotential of 226 mV which induced a current density of 10 mA cm^{-2} with a Tafel slope of 56 mV dec^{-1} during the OER process [100].

As another abundant animal blood protein, hemeproteins containing heme-binding sites are important for metal–ion storage and transport in body fluids. Inspired by these ion interactions, three simple hemeprotein (hemoglobin, myoglobin and c-type cytochromes) coatings were prepared on Ni foam for immobilizing the electrode [101,102]. Among the protein coatings, the film of hemoglobin has a 3D network with nano porous architecture, showing a higher surface activation than the films of hemeprotein, myoglobin and c-type cytochromes. By calculation of specific capacitance based on the weight of protein films, the films of hemoglobin, myoglobin and c-type cytochromes present high specific capacitances of 2052, 1460, and 1213 F g^{-1}, respectively. When the calculation was based on the total weight of electrodes, the three protein-coated Ni foam electrodes showed specific capacitances of 13.8, 8.9 and 8.2 F g^{-1}, respectively.

3.4. Summary

Proteins containing rich functional groups provide abundant interactions with ions. In the precursor solutions of active materials, protein molecules absorbed metal ions and formed the specific nano structures such as hollow sphere, core-shell and particles-incorporated composites, etc. The protein-derived carbon shells/matrices and protein-templated active materials effectively alleviated the negative effect of particle volume expansion during the cycling process of Li-, Na-, K-ion and Li–S batteries. Moreover, the protein-derived active material/carbon composites also generated electrodes with high ionic/electric conductivity, high electrocatalytic activity and large number of active sites due to the large SSAs and good contact with electrolytes, thus, improving their performance of Li-, Na-, K-ion and Li–S batteries, Li-, Zn–air batteries and supercapacitors.

4. Genetically engineered proteins of bio-organisms for electrodes

It is known that protein with specific 3D molecular architectures and peptides sequences are managed by genes providing enormous amounts of coded information. The protein physicochemical properties such as surface residues, dynamical flexibility, packing density, solvent solubility, and the ability to fold/unfold in different environment are highly affected by natural mutations of correspond genes. Based on the natural selections of DNA/RNA level, artificial genetic modifications were developed to expand the proteins with desired properties (e.g., heat/cold stability, ion selectivity, solubility, etc.) of industrial agents. Bacteria and viruses are the organisms with strong reproductive ability and possess a protein coat (membrane proteins). These proteins play an important role in ion absorbing, surface sensing, cell motility and attaching ability in bio-organisms. Applying certain bacteria or viruses, the protein coat can be used as the templates for synthesizing functional materials with specific nanostructures [104]. Moreover, introducing

specific binding units and functional linkers in the coat protein by genetical engineering can help realize the large-scale production of desired materials [105]. The genetically engineered bacteria/viruses including tubular tobacco mosaic virus (TMV), filamentous bacteriophage M13 (with a length of ~860 nm and width of ~6.5 nm) and the recombinant proteins (proteins encoded by recombinant DNA, e.g., collagen, elastin, etc.) were used to direct the formation of active materials for electrodes of Li-ion batteries and Li–air batteries. The performance of genetically engineered protein-derived active materials for electrodes of EESDs is summarized in Table 3.

4.1. Li–ion batteries

Using genetically engineered viruses as templates is considered to be a promising green strategy to prepare the materials with desired nanostructures for anodes of Li–ion batteries [107]. The tobacco mosaic virus (TMV) was genetically modified to introduce the cysteine (Cys) amino acids in the coat protein **(**Fig. 8**a)** [114]. Due to the electrostatic interaction between thiol groups of Cys-and metal ions, the coat protein containing Cys-induced patterning of TMV on a metal matrix [115]. The engineered viruses containing Cys (denoted as TMV1cys) was employed as the templates of Si to prepare multilayered nanoscale 3D-Si anodes with a Ni layer as the current collector (TMV1cys/Ni/Si) [108]. TMV1cys/Ni was fabricated by depositing nickel on the vertically aligned TMV1cys. Then, Si physical vapor deposition (PVD) was applied on TMV1cys/Ni to obtain TMV1cys/Ni/Si (Fig. 8**b, c**). After an annealing process at 350 °C for 1 h in an Ar atmosphere, the TMV1cys/Ni/Si-coated electrode with less impurity and moisture was obtained. When used as the anode of Li-ion batteries, this Si composite achieved a high specific capacity of 3300 mAh g^{-1} and stable cycling performance of 0.2% loss per cycle at 1 C.

In another study, a genetically engineered virus was used to modify cathodes of Li-ion batteries. An M13 virus-based biological toolkit was developed to template the amorphous anhydrous iron phosphate (a-$FePO_4$) [109]. The modified M13 virus (named as E4 virus) has tetraglutamate in the N terminus of pVIII major coat protein. The E4 virus built abundant ionic interactions with metal ions and directed the growth of a-$FePO_4$ (Fig. 8**e**). With the templated a-$FePO_4$ growth on Ag nanoparticles-loaded E4 virus and after an annealing process, the a-$FePO_4$ nanowires with a high electrical conductivity were synthesized. When introducing single-wall carbon nanotubes (SWNTs) in the growth system, the a-$FePO_4$ nanowires fused with SWNTs and formed an a-$FePO_4$/SWNTs hybrid nanostructure (Fig. 8**f, g**). The resulting hybrid showed a specific capacity of 130 mAh g^{-1} at a high rate of 1 C between 1.5 and 4.3 V, which was attributed to the increased electric conductivity of active materials.

Genetically modified bacteria were also studied for modifying transitional metal oxide anodes of Li-ion batteries. For example, *Escherichia coli* bacteria was employed for producing a recombinant protein, ice nucleation protein (INP)-SiliSila, which contains two major functional domains (silicatein-a and silaff). This protein was used as the template by depositing the TiO_2 precursor on the protein surface [110]. After calcination at 600 °C in the air for removing carbon, the nanorod TiO_2 was obtained. In the electrochemical testing, the resulting TiO_2 presented a stable specific capacity of 240 mAh g^{-1} at 1 C. With the same strategy but a different recombinant protein (INP-nR5), a carbon-coated nanorod TiO_2/C was fabricated by a templated TiO_2 deposition and carbonization process [107]. The positively charged 5R5 exhibited interactions with negatively charged TiO_2 and made the *E. coli* cells a framework for TiO_2 nanoparticles. The carbon-coated anatase anode built an excellent specific capacity of 149 mA h g^{-1} at a high rate of 10 C.

The recombinant proteins were prepared by a complex process of bacterial incubation and protein extraction, and were applied to direct the self-assembly of active materials for Li–ion batteries [116]. In a recent study, γ-MnO_2 mesocrystalss with hierarchical hollow microspherical structures were prepared by applying recombinant protein of collagen as the template *via* a hydrothermal method [82]. The obtained γ-MnO_2 mesocrystals showed different sizes of nanospheres when using the collagen with different incubation times and various concentrations. Notably, the γ-MnO_2 mesocrystals have high biocompatibility in the cell, demonstrating their surface modification by the collagen. In another study on employing genetically modified protein, a 3D porous carbon-encapsulated NiSe/Ni_2P composite was prepared *via* freeze-drying and carbonization processes with a recombinant protein (ELP16-His [117]) as the template and carbon source [20]. The polypeptide of epididymal-specific lipocalin (ELP) protein induced the formation of a 3D microporous hydrogel template because of the absorption of Ni^{2+} by the His-tag group that caused a specific cross-link effect. At the current density of 0.1 A g^{-1}, the electrode showed a high specific capacity of 911.3 mAh g^{-1} at the 100th cycle. The other recombinant protein of elastin-like polypeptides named as ELK16-FLAG (The sequence of LELELKLKLELELKLK with a β-sheet-self-assembling architecture), which contains metal-binding motifs, was produced by genetic engineering techniques to direct the assembly of nanoparticles within the crosslinked protein 3D porous matrix [106]. An ionic liquid ($BmimBF_4$) in the formed ELK16-FLAG protein hydrogel served as a fluorine source for F-doped carbon and maintain the porous structure of the protein matrix (Fig. 8**d**). After annealing at 600 °C, the 3D N, F

Table 3
Genetically engineered protein-derived active materials for electrodes of EESDs.

Protein type	Electrode	Systems	Electrochemical performance	Electrolyte	Counter Electrode	Ref.
ELP16-His	3D porous C-encapsulated NiSe/Ni_2P nano- particles	Li–ion	911.3 mA h g^{-1} at 100th cycle, 100 mA g^{-1}	1.0 M $LiPF_6$ in EC/DEC	Li	[20]
		Na–ion	353.6 mA h g^{-1} at 100th cycle, 100 mA g^{-1}	1.0 M $NaClO_4$ in PC + 5% FEC	Na	
ELK16-FLAG	3D porous MnF_2@N,F doped carbon	Li–ion	362 mA h g^{-1} at 0.1C	1 M $LiPF_6$ in EC/DMC	Li	[106]
INP-nR5	Nanostructured TiO_2 anatase	Li–ion	207 mA h g^{-1} after 200 cycles at 1C	1 M $LiPF_6$ in EC/DMC	Li	[107]
TMV1cys	TMV1cys/Ni/Si	Li–ion	3300 mAh/g, 0.2% loss per cycle at 1C	1 M $LiPF_6$ in EC/DEC	Li	[108]
Virus	Templated a-$FePO_4$ nanowires	Li–ion	134 mAh/g at 3C	1 M $LiPF_6$ in EC/DMC	Li	[109]
pET28a	Templated anatase TiO_2	Li–ion	~240 mA h g^{-1} after 30 cycles at 1 C	1 M $LiPF_6$ in EC/DEC	Li	[110]
ELK16-FLAG	MoO_2/Mo_2C@3D N-doped carbon form	Li–air	Round-trip efficiencies 89.1% at 100 mA g^{-1} (2.77–3.11 V)	1 M $LiCF_3SO_3$ in TEGDME	Li	[111]
Virus	Hybrid bio MnO_2 nanowires/Pd nanocatalyst	Li–air	7,340mAh g^{-1} at 0.4 A g^{-1} 8,766 mAh g^{-1} at 0.4 A g^{-1}	0.1 M $LiClO_4$ in DME 1 M $LiCF_3SO_3$ in TEGDME	Li	[112]
GPG-AG3	Pt and Pd nanotubes	Li–air	Low 3.8 V, with round-trip efficiencies of about 65% at a current density of 100 Ma g^{-1}	1 M $LiCF_3SO_3$ in TEGDME	Li	[113]

Notes: EC: ethylene carbonate; DEC: diethyl carbonate; PC: propylene carbonate; FEC: fluoroethylene carbonate; DMC: dimethyl carbonate; DME: dimethoxyethane; TEGDME: tetraethylene glycol dimethyl ether.

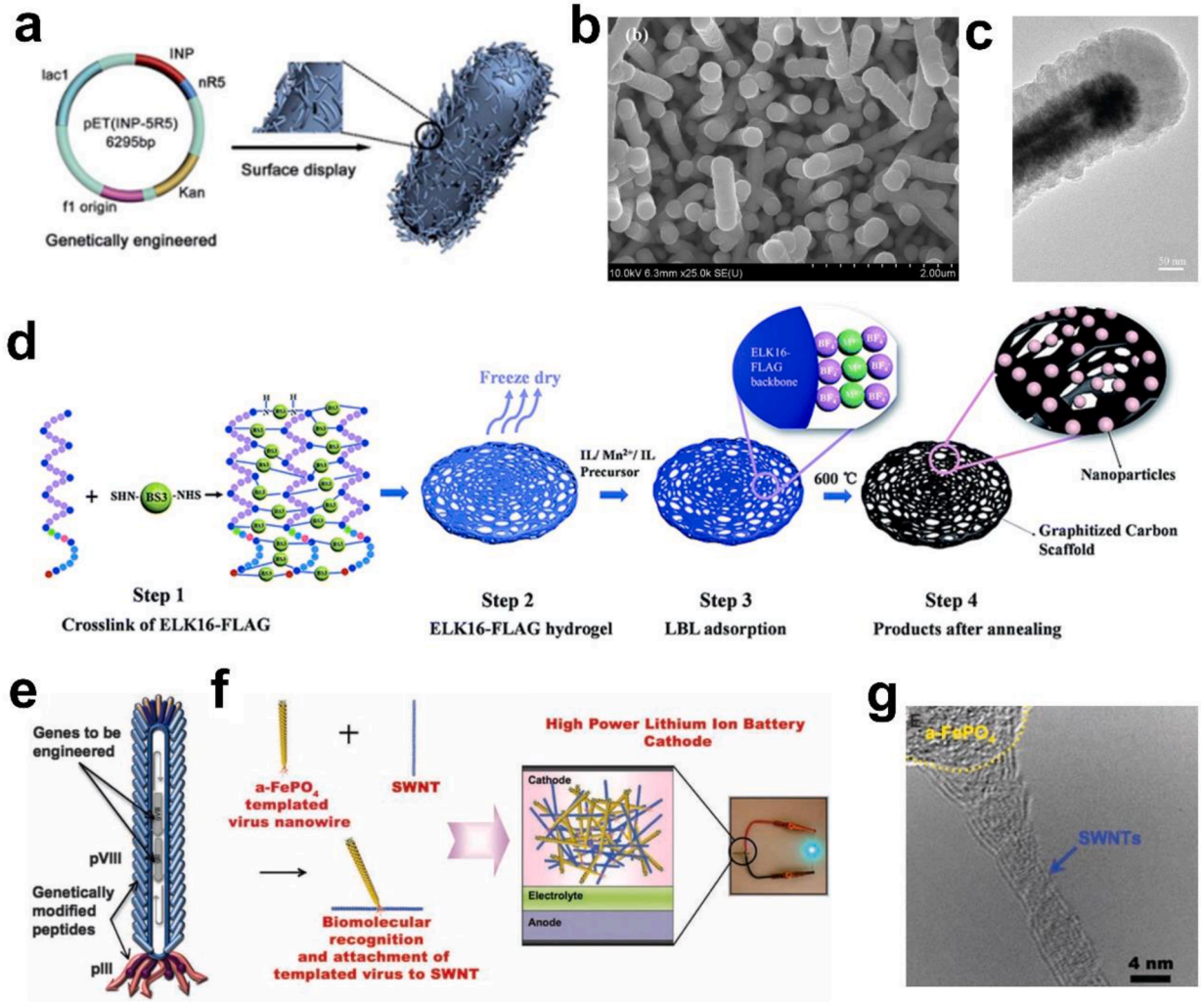

Fig. 8. Protein-modified active materials for Li-ion batteries. (**a**) Schematic of the genetically engineered bacteria surface with recombinant proteins[107]. Copyright 2016, Royal Society of Chemistry. (**b**) SEM image of Ni-coated viruses (TMV1cys) [108]; (**c**) TEM image of Si/Ni coated viruses nanowires (TMV1cys/Ni/Si) [108]. Copyright 2010, American Chemical Society. (**d**) The fabrication of N, F co-doped 3D porous carbon matrix supported MnF_2 nanocrystals with the assistance of recombinant protein (ELK16-FLAG) [106]. Copyright 2016, Royal Society of Chemistry. (**e**) A schematic presentation of genetic engineered M13 viruses is shown with the recombinant protein coat. The gene VIII protein (pVIII), a major capsid protein of the viruses, is modified to serve as a template for a-$FePO_4$ growth, and the gene III protein (pIII) is further engineered to have a binding affinity for SWNTs [109]; (**f**) A schematic diagram for fabricating using genetically engineered viruses [109]; (**g**) The TEM image of the a-$FePO_4$ grown on the genetically engineered viruses/SWNT hybrid nanostructures [109]. Copyright 2009, American Association for the Advancement of Science.

co-coped graphitized carbon-supported MnF_2 nanocrystals (MnF_2@N, F–C) were prepared and showed a high-rate capacity when applied as the anode for Li-ion batteries.

4.2. *Li–air batteries*

Studies on applying genetically engineered bio-organisms (bacteria/viruses) and the resulting recombinant proteins to assist the formation of active materials with desired structures for high-performance Li-air batteries were also reported.

For example, the recombinant protein named ELK16-FLAG was used to modulate the self-assembly of hetero-nanostructured MoO_2/Mo_2C nanocrystals, generating a 3D N-doped carbon matrix for MoO_2/Mo_2C [111]. The as-prepared MoO_2/Mo_2C@N-doped carbon exhibited excellent electrocatalytic activity in both ORR and OER of Li–air batteries, leading to a superior CE of 89.1% (2.77 V/3.11 V) at the current density of 100 mA g^{-1}. This enhanced battery performance was attributed to the hierarchical porous structure of the 3D N-doped carbon and the intimate connection between MoO_2 and Mo_2C nanocrystals. In another study, transition metal-N/C (M-N/C, M = Fe, Co) catalysts were synthesized by the modulation of a recombinant histidine-tag-rich elastin protein (GPG-AG3 ELP) *via* specific metal reduction and post-annealing processes. The water-soluble carbon nanotubes were introduced to be the carbon matrix of electrocatalyst [94]. When applying the M-N/C as the cathode for Li–air batteries, Li_2O_2 nanoparticles were found to firstly form and grow on the protein-decorated area and then on the iron catalyst region during the discharge process. As a result, the cathode with M-N/C exhibited a specific capacity of 800 mAh g^{-1} at a current density of 200 mA g^{-1}, and a CE of ~71.2% with a charge voltage of ~3.65 V. The GPG-AG3 protein fibers with lengths of ~10 μm and diameters of 20–50 nm were also employed to synthesize the Pt and Pd nanotubes which are composed of the packed layers of Pt and Pd nanoparticles (~3–5 nm) [113]. Within the Li-air batteries, the Pt, Pd/C presented a low charge potential of 3.8 V and a CE of ~65% at a current density of 0.1 A g^{-1}.

Virus coat with rich protein binding sites for ions can help the assembly of particles in solutions. M13 virus has five various capsid proteins on the surface and p8 coat protein is the major one. p8 is the

surface protein of the virus, which has two additional negative charged functional groups (-COOH) compared with M13KE (a protein of M13 in which cloning sites have been introduced at the 5' end of gene III). Therefore, the p8 peptides induce rich electrostatic interactions between the manganese ions and virus surfaces. A composite of biotemplated manganese oxide (MO) nanowires with a small content (3 wt%) of incorporated Pd nanoparticles was prepared by using M13 virus as the template. Through a facile aqueous biotemplating nucleation process, the bio-MO nanowires with diameters of ~80 nm and lengths of ~1 mm were obtained [112]. The Pd-incorporated bio-MO nanowires exhibited a high specific capacity of 4,00 mAh g^{-1} at the current density of 1 A g^{-1} and stable cycle life of up to 50 cycles.

4.3. Summary

Genetically engineered proteins possess gene-modulate specific recognition ability for ions, were applied as templates to fabricate the active materials with various nano structures (e.g., as nanowires, nanorods, nanospheres, etc.) *via* a bottom-up methods. Particularly, the bacteria/viruses with a gene-modified protein coat were applied as templates to control the nucleation and growth of active materials (e.g., Si, Ni, MoO_2, a-$FePO_4$, etc.). In addition, the recombinant proteins modified by genetically engineering were applied to direct the self-assembly of active materials (e.g., TiO_2, MoO_2, etc.). These active materials templated by genetically engineered bio-organisms (bacteria/viruses) and their resulting recombinant proteins possess desired configurations of highly dispersed nanoparticles and porous structure with large SSAs, improving the electric/ionic conductivity, cycling stability of Li-ion, Na-ion, and Li–air batteries.

5. Conclusions and perspectives

5.1. Conclusions

Electrochemical energy storage devices (EESDs) are critical to the development of portable electronics, electric vehicles and grid-scale power plants, etc. To meet the requirements of these applications, numerous renewable and low-cost natural resources have been used to build up high performance EESDs. Significantly, various proteins (such as animal proteins, plant proteins, genetically engineered/recombinant proteins, etc.) were reported for advancing performance of EESDs due to their abundant renewable materials with versatile structural characteristics, such as numerous functional groups/heteratoms, interchain bondings and unfoldable quaternary structures. Moreover, protein architectures can be controlled *via* denaturation process to expose more functional groups, making them attractive agents for fabrication of active materials of EESDs. In this review, we have summarized the reported protein-based strategies, which can be categorized into three aspects:

(1) Proteins contain abundant atoms of N, O, S and rich ion-binding sites, thus they were applied to generate heteroatoms-doped activated carbons with porous structures and high SSAs. In Li-, Na-, and K-ion batteries, the doped heteroatoms and porous structures were demonstrated to be able to provide high ionic/electric conductivities and good wetting with electrolytes, improving the specific capacity and cycling performance of electrodes. In metal–air batteries (e.g., Li–air and Zn–air), the doped heteroatoms provided a large number of active sites for catalyzing the OER/ORR in electrodes, which improved the energy density of metal–air batteries and decreases their overpotential. Moreover, in redox flow batteries, the porous defect-rich structures increased the activity and reversibility of the electrochemical reactions. The protein-derived activated carbons with hierarchical porous structures, rich defect and heteroatoms-doped sites also provided a large number of storage sites for charges in supercapacitors, greatly improving the specific capacitance of electrodes.

(2) Proteins are composed of versatile polypeptides possessing abundant amino acids with rich functional groups. These functional groups have strong interactions with ions and inorganic particles, and thus, were used as templates to direct the self-assemblies, modifier of the surfaces or as the hosts of active materials (e.g., Si, MnO_2, MnO, $Ni(OH)_2$, SnO_2, RuO_2, SnSe, TiO_2, MoS_2, CoS_2, $LiFePO_4$, $Li_3V_2(PO_4)_3$, S, nonprecious metal catalysts, etc.) for the electrodes of Li-/Na-ion batteries, Li–S batteries, and metal–air batteries, as well as supercapacitors. With the combination of coprecipitation and carbonization processes, proteins were applied to prepare specific structures or carbon coatings/matrices for the nanoparticles of active materials. In the coprecipitation processes of nanoparticles, the ion binding sites of proteins induced the self-assembly of ions and the formation of a protein layer on the surface of nanoparticles. During the carbonization process, proteins were transformed into a carbon shell/matrix for nanoparticles or removed in air atmosphere. The carbon shell/matrix and the self-assembled porous nanostructures of active materials effectively alleviated the negative effect of particle volume expansion during the cycling processes of alkaline metal-ion batteries. Moreover, the protein-derived shells/matrices and porous structures of active materials also generated electrodes with high ionic/electric conductivity due to the good contact with electrolytes.

(3) Via genetic engineering, the protein polypeptides were modified by the introduction of specific genes into bio-organisms (bacteria/viruses) to generate desired proteins on the surface of the bacteria/viruses. The bacteria/viruses with the designed protein coats were used as effective templates for fabricating nanoparticles with specific morphologies. Moreover, recombinant proteins were used as self-sacrifice matrices by forming protein-based hydrogels to synthesize highly dispersed nanoparticles. These recombinant protein-directed self-assembled active nanoparticles (e.g., NiSe, MnF_2, TiO_2, Si, a-$FePO_4$, MnO_2, MoO_2, Pt/Pd, etc.) presented high SSA, ionic/electric conductivity and porosity, and therefore, effectively improved the electrochemical performance of EESDs.

5.2. Perspectives

Using abundant natural proteins to build the active materials for EESDs is an attractive strategy because of the structural characteristic versatility and abundance of proteins in nature. To develop the protein-derived active materials on improving the performance of EESD electrodes, several issues should be considered during the nanostructure designs: (1) Proteins have natural complex quaternary structures that embed numerous functional groups inside. These functional groups have interactions with ions and particle surfaces when the protein structures are appropriately denatured. The unfolded protein structures of proteins can be controlled by denaturation conditions such as heating, salts, solvents and acid/alkali solutions. Therefore, denaturation processes are not only important for appropriate utilization of the functional groups/heteroatoms of proteins, but also are critical to the directed self-assembly of nanoparticles. (2) Proteins with complex configurations cause difficulty in achieving desired nanostructures. Proteins have dramatic different compositions and physicochemical properties in various precursor solutions of active materials, leading to the mechanism that works for one protein template may not be suitable for another protein. This brings about tremendous challenges for the desirable structure designs based on choosing an appropriate protein template and/or controlled protein denaturation. (3) Using genetically modified bacteria/viruses to produce a recombinant protein with the desired functional groups and architectures are a promising strategy to rationally control structure formation of active materials. Via appropriate

design, protein amino acid sequences may be obtained to induce an oriented self-assembly process, and thus, genetically modified proteins have a great potential to generate high-performance electrodes.

Author contributions

Chenxu Wang: Writing-original draft, Writing - review & editing, Investigation, Conceptualization. **Wei-Hong Zhong:** Writing - review & editing, Supervising, Funding acquisition, Project principle investigator.

Declaration of Competing Interest

The authors declare that they have no known competing financial interests or personal relationships that could have appeared to influence the work reported in this paper.

Data Availability

No data was used for the research described in the article.

Acknowledgments

The authors would like to gratefully acknowledge the financial support by NSF CBET 1929236.

References

[1] M.M. Rahman, A.O. Oni, E. Gemechu, A. Kumar, Assessment of energy storage technologies: a review, Energy Convers. Manag. 223 (2020), 113295, https://doi.org/10.1016/J.ENCONMAN.2020.113295.
[2] M.S. Guney, Y. Tepe, Classification and assessment of energy storage systems, Renew. Sustain. Energy Rev. 75 (2017) 1187–1197, https://doi.org/10.1016/j.rser.2016.11.102.
[3] W. Cao, J. Zhang, H. Li, Batteries with high theoretical energy densities, Energy Storage Mater. 26 (2020) 46–55, https://doi.org/10.1016/j.ensm.2019.12.024.
[4] J.B. Goodenough, M.H. Braga, Batteries for electric road vehicles, Dalt. Trans. 47 (2018) 645–648, https://doi.org/10.1039/c7dt03026f.
[5] A. Masias, J. Marcicki, W.A. Paxton, Opportunities and challenges of lithium ion batteries in automotive applications, ACS Energy Lett. 6 (2021) 621–630, https://doi.org/10.1021/acsenergylett.0c02584.
[6] S. Huang, X. Zhu, S. Sarkar, Y. Zhao, Challenges and opportunities for supercapacitors, APL Mater. 7 (2019) 100901, https://doi.org/10.1063/1.5116146.
[7] M. Zheng, C. Wang, Y. Xu, K. Li, D. Liu, A water-soluble binary conductive binder for Si anode lithium ion battery, Electrochim. Acta 305 (2019) 555–562, https://doi.org/10.1016/j.electacta.2019.02.080.
[8] Y. Wang, Y. Xu, J. Zhou, C. Wang, W. Zhang, Z. Li, F. Guo, H. Chen, H. Zhang, Highly dispersed SnO2 nanoparticles confined on xylem fiber-derived carbon frameworks as anodes for lithium-ion batteries, J. Electroanal. Chem. 879 (2020), 114753, https://doi.org/10.1016/j.jelechem.2020.114753.
[9] C. Wang, X. Yang, M. Zheng, Y. Xu, Synthesis of β-FeOOH nanorods adhered to pine-biomass carbon as a low-cost anode material for Li-ion batteries, J. Alloys Compd. 794 (2019) 569–575, https://doi.org/10.1016/j.jallcom.2019.04.074.
[10] W. Zhang, Y. Xu, H. Li, C. Wang, B. Qin, Z. Li, Y. Chen, K. Jiang, H. Zhang, Incorporating SnO2 nanodots into wood flour-derived hierarchically porous carbon as low-cost anodes for superior lithium storage, J. Electroanal. Chem. 856 (2020), 113654, https://doi.org/10.1016/j.jelechem.2019.113654.
[11] C. Wang, M. Zheng, Y. Xu, D. Wang, D. Liu, Cu ion induced morphology change of hematite microspheres as lithium ion battery anode material by solvothermal synthesis, Ceram. Int. 45 (2019) 2940–2947, https://doi.org/10.1016/j.ceramint.2018.09.222.
[12] T. Li, X. Peng, | Peng Cui, G. Shi, W. Yang, Z. Chen, Y. Huang, | Yongkang Chen, J. Peng, R. Zou, X. Zeng, J. Yu, J. Gan, Z. Mu, Y. Chen, J. Zeng, J. Liu, Y. Yang, Y. Wei, J. Lu, Recent progress and future perspectives of flexible metal-air batteries, SmartMat 2 (2021) 519–553, https://doi.org/10.1002/SMM2.1076.
[13] K. Lourenssen, J. Williams, F. Ahmadpour, R. Clemmer, S. Tasnim, Vanadium redox flow batteries: a comprehensive review, J. Energy Storage 25 (2019), 100844, https://doi.org/10.1016/J.EST.2019.100844.
[14] Y. Wang, X. Wu, Y. Han, T. Li, Flexible supercapacitor: overview and outlooks, J. Energy Storage 42 (2021), 103053, https://doi.org/10.1016/J.EST.2021.103053.
[15] R. Lakra, R. Kumar, P.K. Sahoo, D. Thatoi, A. Soam, A mini-review: graphene based composites for supercapacitor application, Inorg. Chem. Commun. 133 (2021), 108929, https://doi.org/10.1016/j.inoche.2021.108929.
[16] S. Sundriyal, V. Shrivastav, H.D. Pham, S. Mishra, A. Deep, D.P. Dubal, Advances in bio-waste derived activated carbon for supercapacitors: trends, challenges and prospective, Resour. Conserv. Recycl. 169 (2021), 105548, https://doi.org/10.1016/j.resconrec.2021.105548.
[17] H.T. Das, S. Dutta, T.E. Balaji, N. Das, P. Das, N. Dheer, R. Kanojia, P. Ahuja, S. K. Ujjain, Recent trends in carbon nanotube electrodes for flexible supercapacitors: a review of smart energy storage device assembly and performance, Chemosens 10 (2022) 223, https://doi.org/10.3390/CHEMOSENSORS10060223.
[18] M. Zhang, J. Zhang, S. Ran, L. Qiu, W. Sun, Y. Yu, J. Chen, Z. Zhu, A robust bifunctional catalyst for rechargeable Zn-air batteries: ultrathin NiFe-LDH nanowalls vertically anchored on soybean-derived Fe-N-C matrix, Nano Res. 14 (2021) 1175–1186, https://doi.org/10.1007/s12274-020-3168-z.
[19] H.G. Jo, K.H. Kim, H.J. Ahn, Well-dispersed Pt/RuO2-decorated mesoporous N-doped carbon as a hybrid electrocatalyst for Li-O2batteries, RSC Adv. 11 (2021) 12209–12217, https://doi.org/10.1039/d1ra00740h.
[20] J. Yang, N. Yang, Q. Xu, L.S. Pearlie, Y. Zhang, Y. Hong, Q. Wang, W. Wang, Q. Yan, X. Dong, Bioinspired controlled synthesis of NiSe/Ni2P nanoparticles decorated 3D porous carbon for Li/Na ion batteries, ACS Sustain. Chem. Eng. 7 (2019) 13217–13225, https://doi.org/10.1021/acssuschemeng.9b02478.
[21] Y. Zhang, L. Yu, R. Hu, J. Zhang, Y. Wang, R. Niu, X. Qian, J. Zhu, Biomass-derived C/N co-doped Ni(OH)2/NixSy with a sandwich structure for supercapacitors, J. Mater. Chem. A 6 (2018) 17417–17425, https://doi.org/10.1039/c8ta06072j.
[22] M. Mahmoudi, I. Lynch, M.R. Ejtehadi, M.P. Monopoli, F.B. Bombelli, S. Laurent, Protein-nanoparticle interactions: opportunities and challenges, Chem. Rev. 111 (2011) 5610–5637, https://doi.org/10.1021/cr100440g.
[23] S. Lin, X. Fu, M. Luo, C. Wang, W.H. Zhong, Interface-tailored forces fluffing protein fiber membranes for high-performance filtration, Sep. Purif. Technol. 278 (2022), 119570, https://doi.org/10.1016/j.seppur.2021.119570.
[24] C. Wang, X. Fu, C. Ying, J. Liu, W. Zhong, Natural protein as novel additive of a commercial electrolyte for Long-Cycling lithium metal batteries, Chem. Eng. J. 437 (2022), 135283, https://doi.org/10.1016/j.cej.2022.135283.
[25] C. Wang, X. Fu, S. Lin, J. Liu, W.H. Zhong, A protein-enabled protective film with functions of self-adapting and anion-anchoring for stabilizing lithium-metal batteries, J. Energy Chem. 64 (2021) 485–495, https://doi.org/10.1016/j.jechem.2021.05.014.
[26] C. Wang, R. Odstrcil, J. Liu, W.-.H. Zhong, Protein-modified SEI formation and evolution in Li metal batteries, J. Energy Chem. 73 (2022) 248–258, https://doi.org/10.1016/j.jechem.2022.06.017.
[27] Y.S. Yun, S.Y. Cho, J. Shim, B.H. Kim, S.J. Chang, S.J. Baek, Y.S. Huh, Y. Tak, Y. W. Park, S. Park, H.J. Jin, Microporous carbon nanoplates from regenerated silk proteins for supercapacitors, Adv. Mater. 25 (2013) 1993–1998, https://doi.org/10.1002/ADMA.201204692.
[28] I.M. Mosa, A. Pattammattel, K. Kadimisetty, P. Pande, M.F. El-Kady, G.W. Bishop, M. Novak, R.B. Kaner, A.K. Basu, C.V. Kumar, J.F. Rusling, Ultrathin graphene–protein supercapacitors for miniaturized bioelectronics, Adv. Energy Mater. 7 (2017), 1700358, https://doi.org/10.1002/AENM.201700358.
[29] M. Chen, X. Fu, Z. Chen, J. Liu, W.H. Zhong, Protein-engineered functional materials for bioelectronics, Adv. Funct. Mater. 31 (2021) 1–25, https://doi.org/10.1002/adfm.202006744.
[30] S. Guo, Y. Chen, L. Shi, Y. Dong, J. Ma, X. Chen, H. Song, Nitrogen-doped biomass-based ultra-thin carbon nanosheets with interconnected framework for high-performance lithium-ion batteries, Appl. Surf. Sci. 437 (2018) 136–143, https://doi.org/10.1016/j.apsusc.2017.12.144.
[31] D. Zhang, G. Wang, L. Xu, J. Lian, J. Bao, Y. Zhao, J. Qiu, H. Li, Defect-rich N-doped porous carbon derived from soybean for high rate lithium-ion batteries, Appl. Surf. Sci. 451 (2018) 298–305, https://doi.org/10.1016/j.apsusc.2018.04.251.
[32] Y. Zhang, Y. Wang, Y. Meng, G. Tan, Y. Guo, D. Xiao, Porous nitrogen-doped carbon tubes derived from reed catkins as a high-performance anode for lithium ion batteries, RSC Adv. 6 (2016) 98434–98439, https://doi.org/10.1039/c6ra21620j.
[33] J. Zhao, X. Wen, H. Xu, Y. Wen, H. Lu, X. Meng, Salting-out and salting-in of protein: a novel approach toward fabrication of hierarchical porous carbon for energy storage application, J. Alloys Compd. 788 (2019) 397–406, https://doi.org/10.1016/j.jallcom.2019.02.252.
[34] X. Liu, M. Wen, Y. Zhao, Y. Dong, Q. Fan, Q. Kuang, Q. Li, Cheese-like bulk carbon with nanoholes prepared from egg white as an anode material for lithium and sodium ion batteries, RSC Adv. 6 (2016) 80986–80993, https://doi.org/10.1039/c6ra16905h.
[35] J. Choi, M.E. Lee, S. Lee, H.J. Jin, Y.S. Yun, Pyroprotein-derived hard carbon fibers exhibiting exceptionally high plateau capacities for sodium ion batteries, ACS Appl. Energy Mater. 2 (2019) 1185–1191, https://doi.org/10.1021/acsaem.8b01734.
[36] J. Sun, Y. Sun, J.A.S. Oh, Q. Gu, W. Zheng, M. Goh, K. Zeng, Y. Cheng, L. Lu, Insight into the structure-capacity relationship in biomass derived carbon for high-performance sodium-ion batteries, J. Energy Chem. 62 (2021) 497–504, https://doi.org/10.1016/j.jechem.2021.04.009.
[37] Y. Sun, Q. Wu, Y. Wang, C. Li, X. Liang, H. Xiang, Protein-derived 3D amorphous carbon with N, O doping as high rate and long lifespan anode for potassium ion batteries, J. Power Sources 512 (2021), 230530, https://doi.org/10.1016/j.jpowsour.2021.230530.
[38] H.G. Jo, H.J. Ahn, Accelerating the oxygen reduction reaction and oxygen evolution reaction activities of n and p co-doped porous activated carbon for li-o2 batteries, Catalysts 10 (2020) 1–13, https://doi.org/10.3390/catal10111316.
[39] C. Wang, N.H. Xie, Y. Zhang, Z. Huang, K. Xia, H. Wang, S. Guo, B.Q. Xu, Y. Zhang, Silk-derived highly active oxygen electrocatalysts for flexible and

rechargeable Zn-Air batteries, Chem. Mater. 31 (2019) 1023–1029, https://doi.org/10.1021/acs.chemmater.8b04572.
[40] M. Hao, R. Dun, Y. Su, L. He, F. Ning, X. Zhou, W. Li, In situ self-doped biomass-derived porous carbon as an excellent oxygen reduction electrocatalyst for fuel cells and metal-air batteries, J. Mater. Chem. A 9 (2021) 14331–14343, https://doi.org/10.1039/d1ta01417j.
[41] M.E. Lee, D. Jang, S. Lee, J. Yoo, J. Choi, H.J. Jin, S. Lee, S.Y. Cho, Silk protein-derived carbon fabric as an electrode with high electro-catalytic activity for all-vanadium redox flow batteries, Appl. Surf. Sci. 567 (2021), 150810, https://doi.org/10.1016/j.apsusc.2021.150810.
[42] R. Wang, Y. Li, Twin-cocoon-derived self-standing nitrogen-oxygen-rich monolithic carbon material as the cost-effective electrode for redox flow batteries, J. Power Sources 421 (2019) 139–146, https://doi.org/10.1016/j.jpowsour.2019.03.023.
[43] H. Chen, L. Zhang, H. Wang, D. Sui, F. Meng, W. Qi, Synergetic modulation of graphene oxide and metal oxide particles for exploring integrated capacitance of milk colloid-derived carbon, Colloids Surf. A Physicochem. Eng. Asp. 608 (2021), 125599, https://doi.org/10.1016/j.colsurfa.2020.125599.
[44] I. Denmark, A. Khan, T. Scifres, T. Viswanathan, F. Watanabe, N. Siraj, Synthesis and characterization of supercapacitor materials from soy, Electrochem 2 (2021) 534–545, https://doi.org/10.3390/electrochem2040034.
[45] J. Zhang, J. Li, Y. Yan, A. Li, L. Ren, The porous carbon derived from soy protein isolate “tofu” with electrochemical performance controlled by external pressure, J. Electroanal. Chem. 887 (2021), 115174, https://doi.org/10.1016/j.jelechem.2021.115174.
[46] D. Lv, T. Zhang, D. Wang, J. Li, L. Wang, One-pot synthesis of nitrogen-doped carbon aerogels derived from sodium lignosulfonate embedded in carrageenan for supercapacitor electrode materials, Ind. Crops Prod. 170 (2021), 113750, https://doi.org/10.1016/j.indcrop.2021.113750.
[47] Y. Ding, Y. Li, Y. Dai, X. Han, B. Xing, L. Zhu, K. Qiu, S. Wang, A novel approach for preparing in-situ nitrogen doped carbon via pyrolysis of bean pulp for supercapacitors, Energy 216 (2021), 119227, https://doi.org/10.1016/j.energy.2020.119227.
[48] J. Yu, X. Li, Z. Cui, D. Chen, X. Pang, Q. Zhang, F. Shao, H. Dong, L. Yu, L. Dong, Tailoring in-situ N, O, P, S-doped soybean-derived porous carbon with ultrahigh capacitance in both acidic and alkaline media, Renew. Energy 163 (2021) 375–385, https://doi.org/10.1016/j.renene.2020.08.066.
[49] J. Yang, Z. Tan, X. Chen, Y. Liang, M. Zheng, H. Hu, H. Dong, X. Liu, Y. Liu, Y. Xiao, A mild method to prepare nitrogen-rich interlaced porous carbon nanosheets for high-performance supercapacitors, J. Colloid Interface Sci. 599 (2021) 381–389, https://doi.org/10.1016/j.jcis.2021.04.119.
[50] L. Lin, H. Xie, Y. Lei, R. Li, X. Liu, J. Ou, Nitrogen source-mediated cocoon silk-derived N, O-doped porous carbons for high performance symmetric supercapacitor, J. Mater. Sci. Mater. Electron. 31 (2020) 10825–10835, https://doi.org/10.1007/s10854-020-03634-x.
[51] Y. Wen, X. Liu, X. Wen, X. Chen, K. Szymańska, R. Dobrzyńska, E. Mijowska, Na3PO4 assistant dispersion of nano-CaCO3 template to enhance electrochemical interface: N/O/P co-doped porous carbon hybrids towards high-performance flexible supercapacitors, Compos. Part B Eng. 199 (2020), https://doi.org/10.1016/j.compositesb.2020.108256.
[52] P. Li, H. Xie, Y. Liu, J. Wang, X. Wang, Y. Xie, W. Hu, T. Xie, Y. Wang, Y. Zhang, Dual-templated 3D nitrogen-enriched hierarchical porous carbon aerogels with interconnected carbon nanosheets from self-assembly natural biopolymer gel for supercapacitors, Electrochim. Acta 353 (2020), 136514, https://doi.org/10.1016/j.electacta.2020.136514.
[53] Z. Ma, Z. Zhang, Y. Qu, F. Lai, Q. Li, X. Wu, Q. Wu, Q. Li, H. Wang, Y. Huang, Yeast protein derived hierarchical mesoporous carbon for symmetrical capacitor with excellent electrochemical performances, Microporous Mesoporous Mater. 281 (2019) 50–56, https://doi.org/10.1016/j.micromeso.2019.02.013.
[54] M. Demir, B. Ashourirad, J.H. Mugumya, S.K. Saraswat, H.M. El-Kaderi, R. B. Gupta, Nitrogen and oxygen dual-doped porous carbons prepared from pea protein as electrode materials for high performance supercapacitors, Int. J. Hydrogen Energy 43 (2018) 18549–18558, https://doi.org/10.1016/j.ijhydene.2018.03.220.
[55] P. Song, X. Shen, W. He, L. Kong, X. He, Z. Ji, A. Yuan, G. Zhu, N. Li, Protein-derived nitrogen-doped hierarchically porous carbon as electrode material for supercapacitors, J. Mater. Sci. Mater. Electron. 29 (2018) 12206–12215, https://doi.org/10.1007/s10854-018-9329-0.
[56] B. Niu, M. Yuan, F. Jiang, M. Li, Protein powder derived porous carbon materials as supercapacitor electrodes, Int. J. Electrochem. Sci. 14 (2019) 3253–3264, https://doi.org/10.20964/2019.04.33.
[57] J. Yang, Y. Wang, J. Luo, L. Chen, Highly nitrogen-doped graphitic carbon fibers from sustainable plant protein for supercapacitor, Ind. Crops Prod. 121 (2018) 226–235, https://doi.org/10.1016/j.indcrop.2018.05.013.
[58] J. Yang, Y. Wang, J. Luo, L. Chen, Facile preparation of self-standing hierarchical porous nitrogen-doped carbon fibers for supercapacitors from plant protein-lignin electrospun fibers, ACS Omega 3 (2018) 4647–4656, https://doi.org/10.1021/acsomega.7b01876.
[59] J. Sun, J. Niu, M. Liu, J. Ji, M. Dou, F. Wang, Biomass-derived nitrogen-doped porous carbons with tailored hierarchical porosity and high specific surface area for high energy and power density supercapacitors, Appl. Surf. Sci. 427 (2018) 807–813, https://doi.org/10.1016/j.apsusc.2017.07.220.
[60] S.W. Xu, Y.Q. Zhao, Y.X. Xu, Q.H. Chen, G.Q. Zhang, Q.Q. Xu, D.D. Zhao, X. Zhang, C.L. Xu, Heteroatom doped porous carbon sheets derived from protein-rich wheat gluten for supercapacitors: the synergistic effect of pore properties and heteroatom on the electrochemical performance in different electrolytes, J. Power Sources 401 (2018) 375–385, https://doi.org/10.1016/j.jpowsour.2018.09.012.
[61] L. Shi, L. Jin, Z. Meng, Y. Sun, C. Li, Y. Shen, A novel porous carbon material derived from the byproducts of bean curd stick manufacture for high-performance supercapacitor use, RSC Adv. 8 (2018) 39937–39947, https://doi.org/10.1039/C8RA08664H.
[62] H. Zhao, B. Xing, C. Zhang, G. Huang, Q. Liu, G. Yi, J. Jia, M. Ma, Z. Chen, C. Zhang, Efficient synthesis of nitrogen and oxygen co-doped hierarchical porous carbons derived from soybean meal for high-performance supercapacitors, J. Alloys Compd. 766 (2018) 705–715, https://doi.org/10.1016/j.jallcom.2018.06.267.
[63] H. Ma, C. Li, M. Zhang, J.D. Hong, G. Shi, Graphene oxide induced hydrothermal carbonization of egg proteins for high-performance supercapacitors, J. Mater. Chem. A 5 (2017) 17040–17047, https://doi.org/10.1039/c7ta04771a.
[64] B. Li, F. Dai, Q. Xiao, L. Yang, J. Shen, C. Zhang, M. Cai, B. Li, C.M. Zhang, F. Dai, Q.F. Xiao, L. Yang, M. Cai, J. Shen, Activated carbon from biomass transfer for high-energy density lithium-ion supercapacitors, Adv. Energy Mater. 6 (2016), 1600802, https://doi.org/10.1002/AENM.201600802.
[65] C. Long, J. Zhuang, Y. Xiao, M. Zheng, H. Hu, H. Dong, B. Lei, H. Zhang, Y. Liu, Nitrogen-doped porous carbon with an ultrahigh specific surface area for superior performance supercapacitors, J. Power Sources 310 (2016) 145–153, https://doi.org/10.1016/j.jpowsour.2016.01.052.
[66] S.Y. Cho, H.J. Yoon, N.R. Kim, Y.S. Yun, H.J. Jin, Sodium-ion supercapacitors based on nanoporous pyroproteins containing redox-active heteroatoms, J. Power Sources 329 (2016) 536–545, https://doi.org/10.1016/j.jpowsour.2016.08.114.
[67] M. Xu, Q. Huang, R. Sun, X. Wang, Simultaneously obtaining fluorescent carbon dots and porous active carbon for supercapacitors from biomass, RSC Adv. 6 (2016) 88674–88682, https://doi.org/10.1039/c6ra18725k.
[68] Q. Xie, R. Bao, A. Zheng, Y. Zhang, S. Wu, C. Xie, P. Zhao, Sustainable low-cost green electrodes with high volumetric capacitance for aqueous symmetric supercapacitors with high energy density, ACS Sustain. Chem. Eng. 4 (2016) 1422–1430, https://doi.org/10.1021/acssuschemeng.5b01417.
[69] K. Wang, Y. Cao, X. Wang, P.R. Kharel, W. Gibbons, B. Luo, Z. Gu, Q. Fan, L. Metzger, Nickel catalytic graphitized porous carbon as electrode material for high performance supercapacitors, Energy 101 (2016) 9–15, https://doi.org/10.1016/j.energy.2016.01.059.
[70] Y. Wang, Y. Song, Y. Wang, X. Chen, Y. Xia, Z. Shao, Graphene/silk fibroin based carbon nanocomposites for high performance supercapacitors, J. Mater. Chem. A 3 (2015) 773–781, https://doi.org/10.1039/c4ta04772a.
[71] M. Wahid, G. Parte, D. Phase, S. Ogale, Yogurt: a novel precursor for heavily nitrogen doped supercapacitor carbon, J. Mater. Chem. A 3 (2015) 1208–1215, https://doi.org/10.1039/c4ta06068g.
[72] J. Hou, C. Cao, F. Idrees, X. Ma, Hierarchical porous nitrogen-doped carbon nanosheets derived from silk for ultrahigh-capacity battery anodes and supercapacitors, ACS Nano 9 (2015) 2556–2564, https://doi.org/10.1021/nn506394r.
[73] Y.S. Yun, S.Y. Cho, H.J. Jin, Carbon aerogels based on regenerated silk proteins and graphene oxide for supercapacitors, Macromol. Res. 22 (2014) 509–514, https://doi.org/10.1007/s13233-014-2071-4.
[74] Z. Li, Z. Xu, X. Tan, H. Wang, C.M.B. Holt, T. Stephenson, B.C. Olsen, D. Mitlin, Mesoporous nitrogen-rich carbons derived from protein for ultra-high capacity battery anodes and supercapacitors, Energy Environ. Sci. 6 (2013) 871–878, https://doi.org/10.1039/c2ee23599d.
[75] B. Xu, S. Hou, G. Cao, F. Wu, Y. Yang, Sustainable nitrogen-doped porous carbon with high surface areas prepared from gelatin for supercapacitors, J. Mater. Chem. 22 (2012) 19088–19093, https://doi.org/10.1039/c2jm32759g.
[76] J. Chen, Y. Liu, W. Li, L. Xu, H. Yang, C.M. Li, Nitrogen-enriched carbon sheets derived from egg white by using expanded perlite template and its high-performance supercapacitors, Nanotechnology 26 (2015), https://doi.org/10.1088/0957-4484/26/34/345401.
[77] H. Zhou, Y. Zhou, L. Li, Y. Li, X. Liu, P. Zhao, B. Gao, Amino acid protic ionic liquids: multifunctional carbon precursor for n/s codoped hierarchically porous carbon materials toward supercapacitive energy storage, ACS Sustain. Chem. Eng. 7 (2019) 9281–9290, https://doi.org/10.1021/acssuschemeng.9b00279.
[78] S. Unknown, P. Chand, A. Joshi, Biomass derived carbon for supercapacitor applications: review, J. Energy Storage 39 (2021), 102646, https://doi.org/10.1016/j.est.2021.102646.
[79] H. Qu, Y. Zhou, Y. Ma, P. Zhao, B. Gao, M. Guo, C. Feng, A green catalyst for hydrolysis of cellulose: amino acid protic ionic liquid, J. Taiwan Inst. Chem. Eng. 93 (2018) 667–673, https://doi.org/10.1016/j.jtice.2018.09.024.
[80] T. Wang, F. Wu, W. Yang, X. Dai, Facile fabrication of hierarchical porous silicon/N-doped carbon composites via biomass fermentation treatment for high-performance lithium-ion batteries, J. Alloys Compd. 898 (2022), 162781, https://doi.org/10.1016/j.jallcom.2021.162781.
[81] X. Xu, F. Wu, W. Yang, X. Dai, T. Wang, J. Zhou, J. Wang, D. Guo, Silicon@natural nitrogen-doped biomass carbon composites derived from “silicon Tofu” as green and efficient anode materials for lithium-ion batteries, ACS Sustain. Chem. Eng. (2021), https://doi.org/10.1021/acssuschemeng.1c03879.
[82] H. He, C. Fu, Y. An, J. Feng, J. Xiao, Biofunctional hollow γ-MnO2microspheres by a one-pot collagen-templated biomineralization route and their applications in lithium batteries, RSC Adv. 11 (2021) 37040–37048, https://doi.org/10.1039/d1ra06899g.
[83] Y. Zhang, X. Song, R. Huang, Y. Ye, F. Cheng, H. Li, A sustainable route from kelp to a porous MnO/C network anode for high-capacity lithium-ion batteries, J. Mater. Sci. 55 (2020) 10740–10750, https://doi.org/10.1007/s10853-020-04680-w.

[84] J. Ou, L. Yang, F. Jin, S. Wu, J. Wang, High performance of LiFePO4 with nitrogen-doped carbon layers for lithium ion batteries, Adv. Powder Technol. 31 (2020) 1220–1228, https://doi.org/10.1016/j.apt.2019.12.044.
[85] X. Meng, D. Deng, Bio-inspired synthesis of 3-D network of NiO-Ni nanowires on carbonized eggshell membrane for lithium-ion batteries, Chem. Eng. Sci. 194 (2019) 134–141, https://doi.org/10.1016/j.ces.2018.06.038.
[86] Y. Li, K. Xiang, C. Shi, W. Zhou, Y. Zhu, H. Chen, Frogegg-like Li3V2(PO4)3/carbon composite with three dimensional porous structure and its improved electrochemical performance in lithium ion batteries, Mater. Lett. 204 (2017) 104–107, https://doi.org/10.1016/j.matlet.2017.05.098.
[87] X. Wang, J. Li, Z. Chen, L. Lei, X. Liao, X. Huang, B. Shi, Hierarchically structured C@SnO2@C nanofiber bundles with high stability and effective ambipolar diffusion kinetics for high-performance Li-ion batteries, J. Mater. Chem. A 4 (2016) 18783–18791, https://doi.org/10.1039/c6ta06622d.
[88] L. Wang, D. Wang, Z. Dong, F. Zhang, J. Jin, Interface chemistry engineering of protein-directed SnO2 nanocrystal-based anode for lithium-ion batteries with improved performance, Small 10 (2014) 998–1007, https://doi.org/10.1002/smll.201300843.
[89] J. Zhang, Y. Cai, Q. Zhong, D. Lai, J. Yao, Porous nitrogen-doped carbon derived from silk fibroin protein encapsulating sulfur as a superior cathode material for high-performance lithium-sulfur batteries, Nanoscale 7 (2015) 17791–17797, https://doi.org/10.1039/c5nr04768d.
[90] X. Chen, G. Du, M. Zhang, A. Kalam, Q. Su, S. Ding, B. Xu, Nitrogen-doped hierarchical porous carbon derived from low-cost biomass pomegranate residues for high performance lithium-sulfur batteries, J. Electroanal. Chem. 848 (2019), 113316, https://doi.org/10.1016/j.jelechem.2019.113316.
[91] G. Ren, S. Li, Z.X. Fan, J. Warzywoda, Z. Fan, Soybean-derived hierarchical porous carbon with large sulfur loading and sulfur content for high-performance lithium-sulfur batteries, J. Mater. Chem. A 4 (2016) 16507–16515, https://doi.org/10.1039/c6ta07446d.
[92] J. Wu, J. Hu, K. Song, J. Xu, H. Gao, Spirulina-derived nitrogen-doped porous carbon as carbon/S composite cathodes for high cyclability lithium-sulphur batteries, J. Alloys Compd. 704 (2017) 1–6, https://doi.org/10.1016/j.jallcom.2017.02.052.
[93] J.S. Lee, H.S. Kim, W.H. Ryu, Iron/carbon composite microfiber catalyst derived from hemoglobin blood protein for lithium-oxygen batteries, Appl. Surf. Sci. 466 (2019) 562–567, https://doi.org/10.1016/j.apsusc.2018.10.023.
[94] G. Guo, X. Yao, H. Ang, H. Tan, Y. Zhang, Y. Guo, E. Fong, Q. Yan, Using elastin protein to develop highly efficient air cathodes for lithium-O2 batteries, Nanotechnology 27 (2015), https://doi.org/10.1088/0957-4484/27/4/045401.
[95] P. Kong, L. Zhu, F. Li, G. Xu, Self-supporting electrode composed of SnSe nanosheets, thermally treated protein, and reduced graphene oxide with enhanced pseudocapacitance for advanced sodium-ion batteries, ChemElectroChem 6 (2019) 5642–5650, https://doi.org/10.1002/celc.201901517.
[96] R. Yang, L. Sun, W. Liu, Y. Zhang, Y. Cui, Y. Du, S. Liu, H. Wang, M. Huang, Bio-derived 3D TiO2 hollow spheres with a mesocrystal nanostructure to achieve improved electrochemical performance of Na-ion batteries in ether-based electrolytes, J. Mater. Chem. A 7 (2019) 3399–3407, https://doi.org/10.1039/c9ta00334g.
[97] H.S. Kim, J. Lee, J.H. Jang, H. Jin, V.K. Paidi, S.H. Lee, K.S. Lee, P. Kim, S.J. Yoo, Waste pig blood-derived 2D Fe single-atom porous carbon as an efficient electrocatalyst for zinc–air batteries and AEMFCs, Appl. Surf. Sci. 563 (2021), 150208, https://doi.org/10.1016/j.apsusc.2021.150208.
[98] M.K. Puglia, M. Malhotra, A. Chivukula, C.V. Kumar, simple-Stir" Heterolayered MoS2/Graphene Nanosheets for Zn-Air Batteries, ACS Appl. Nano Mater. 4 (2021) 10389–10398, https://doi.org/10.1021/acsanm.1c01792.
[99] M.E. Lee, N.R. Kim, M.Y. Song, H.J. Jin, Microporous carbon nanoplate/amorphous ruthenium oxide hybrids as supercapacitor electrodes, J. Nanosci. Nanotechnol. 16 (2016) 10431–10436, https://doi.org/10.1166/jnn.2016.13173.
[100] B. Li, R. Xing, S.V. Mohite, S.S. Latthe, A. Fujishima, S. Liu, Y. Zhou, CoS2 nanodots anchored into heteroatom-doped carbon layer via a biomimetic strategy: boosting the oxygen evolution and supercapacitor performance, J. Power Sources 436 (2019), 226862, https://doi.org/10.1016/j.jpowsour.2019.226862.
[101] M. Khairy, S.A. El-Safty, Promising supercapacitor electrodes based immobilization of proteins onto macroporous Ni foam materials, J. Energy Chem. 24 (2015) 31–38, https://doi.org/10.1016/S2095-4956(15)60281-9.
[102] M. Khairy, S.A.E.L. Safty, Hemoproteins-nickel foam hybrids as effective supercapacitors, Chem. Commun. 50 (2014) 1356–1358, https://doi.org/10.1039/c3cc48155g.
[103] A.F. Gonzalez, N.H. Yang, R.S. Liu, Silicon anode design for lithium-ion batteries: progress and perspectives, J. Phys. Chem. C 121 (2017) 27775–27787, https://doi.org/10.1021/acs.jpcc.7b07793.
[104] R.M. Kramer, C. Li, D.C. Carter, M.O. Stone, R.R. Naik, Engineered protein cages for nanomaterial synthesis, J. Am. Chem. Soc. 126 (2004) 13282–13286, https://doi.org/10.1021/JA046735B/SUPPL_FILE/JA046735BSI20040909_045250.PDF.
[105] L. Shen, N. Bao, Z. Zhou, P.E. Prevelige, A. Gupta, Materials design using genetically engineered proteins, J. Mater. Chem. 21 (2011) 18868–18876, https://doi.org/10.1039/c1jm12238j.
[106] Y. Lu, Y.P. Zhou, Q.Y. Yan, E. Fong, Bio-inspired synthesis of N,F co-doped 3D graphitized carbon foams containing manganese fluoride nanocrystals for lithium ion batteries, J. Mater. Chem. A 4 (2016) 2691–2698, https://doi.org/10.1039/c5ta09185c.
[107] H. Ping, H. Xie, M. Xiang, B.L. Su, Y. Wang, J. Zhang, F. Zhang, Z. Fu, Confined-space synthesis of nanostructured anatase, directed by genetically engineered living organisms for lithium-ion batteries, Chem. Sci. 7 (2016) 6330–6336, https://doi.org/10.1039/c6sc02311h.
[108] X. Chen, K. Gerasopoulos, J. Guo, A. Brown, C. Wang, R. Ghodssi, J.N. Culver, Virus-enabled silicon anode for lithium-ion batteries, ACS Nano 4 (2010) 5366–5372, https://doi.org/10.1021/nn100963j.
[109] J.P. Breen, F.C. Meunier, M. Haneda, W. Sun, Y. Kindaichi, H. Hamada, Y. Yu, J. Saussey, M. Daturi, C. Hedouin, T. Seguelong, A. Simon, J.M. Weil, G.W. Harris, H. Frei, B. Weckhuysen, S. Diego, E. Fridell, M. Wolf, D. a King, Z.P. Liu, H. Arnolds, I.M. Lane, D.C. Papageorgopoulos, A. Rushton, M. Gill, P. Fox, A. Daunois, M. Yamaguchi, I. Goto, M. Kumagai, K.C. Patil, M.S. Hegde, S. J. Jenkins, P. Bazin, O. Marie, D. Astruc, T. Yoshinari, Y. Kintaichi, Y.J. Lee, H. Yi, W.-J. Kim, K. Kang, D.S. Yun, M.S. Strano, G. Ceder, A.M. Belcher, Fabricating genetically engineered high-power lithium-ion batteries using multiple virus genes, Sci. NY 324 (2009) 1051–1055. http://www.sciencemag.org/content/324/5930/1051.
[110] S.H. Xue, H. Xie, H. Ping, X.M. Xu, J. Li, X.Y. Yang, Z.Y. Fu, B.L. Su, Controlled synthesis of mesoporous nanostructured anatase TiO2 on a genetically modified Escherichia coli surface for high reversible capacity and long-life lithium-ion batteries, RSC Adv. 6 (2016) 59422–59428, https://doi.org/10.1039/c6ra09974b.
[111] Y. Lu, H. Ang, Q. Yan, E. Fong, Bioinspired synthesis of hierarchically porous MoO2/Mo2C nanocrystal decorated N-doped carbon foam for lithium-oxygen batteries, Chem. Mater. 28 (2016) 5743–5752, https://doi.org/10.1021/acs.chemmater.6b01966.
[112] D. Oh, J. Qi, Y.C. Lu, Y. Zhang, Y. Shao-Horn, A.M. Belcher, Biologically enhanced cathode design for improved capacity and cycle life for lithium-oxygen batteries, Nat. Commun. 4 (2013) 4–11, https://doi.org/10.1038/ncomms3756.
[113] G. Guo, T.H.A. Truong, H. Tan, H. Ang, W. Zhang, C. Xu, X. Rui, Z. Hu, E. Fong, Q. Yan, Platinum and palladium nanotubes based on genetically engineered elastin-mimetic fusion protein-fiber templates: synthesis and application in lithium-O2 batteries, Chem. - An Asian J. 9 (2014) 2555–2559, https://doi.org/10.1002/asia.201402191.
[114] K. Gerasopoulos, M. McCarthy, E. Royston, J.N. Culver, R. Ghodssi, Nanostructured nickel electrodes using the Tobacco mosaic virus for microbattery applications, J. Micromech. Microeng. 18 (2008), 104003, https://doi.org/10.1088/0960-1317/18/10/104003.
[115] E. Royston, A. Ghosh, P. Kofinas, M.T. Harris, J.N. Culver, Self-assembly of virus-structured high surface area nanomaterials and their application as battery electrodes, Langmuir 24 (2008) 906–912, https://doi.org/10.1021/la7016424.
[116] Y.Y. Peng, A. Yoshizumi, S.J. Danon, V. Glattauer, O. Prokopenko, O. Mirochnitchenko, Z. Yu, M. Inouye, J.A. Werkmeister, B. Brodsky, J.A. M. Ramshaw, A Streptococcus pyogenes derived collagen-like protein as a non-cytotoxic and non-immunogenic cross-linkable biomaterial, Biomaterials 31 (2010) 2755–2761, https://doi.org/10.1016/j.biomaterials.2009.12.040.
[117] Y. Zhou, W. Sun, X. Rui, Y. Zhou, W.J. Ng, Q. Yan, E. Fong, Biochemistry-derived porous carbon-encapsulated metal oxide nanocrystals for enhanced sodium storage, Nano Energy 21 (2016) 71–79, https://doi.org/10.1016/j.nanoen.2015.12.003.

Chenxu Wang is a Ph.D. candidate in the School of Mechanical and Materials Engineering at Washington State University, USA. He received his M.S. degree in Material Science and Engineering from East China University of Science and Technology, China, in 2019 and worked as battery electrolyte engineer in REPT BATTERO Energy Co., Ltd. from 2019 to 2020. His research interests focus on functional materials for components of lithium batteries.

Wei-Hong Zhong is an endowed chair professor, Westinghouse Distinguished Professor in the School of Mechanical and Materials at Washington State University, USA. Her current research interests include polymer composites, biomaterials, and nanotechnology for energy storage and environment applications.